12-2007

Flow Structures in an Enclosed Simplified Full Scale Under-hood Engine Compartment during Steady State Operation

Chin Hoong Leong

FLOW STRUCTURES IN AN ENCLOSED SIMPLIFIED FULL SCALE UNDER-HOOD ENGINE COMPARTMENT DURING STEADY STATE OPERATION

by

Chin Hoong Leong

A Thesis
Submitted to the
Faculty of The Graduate College
in partial fulfillment of the
requirements for the
Degree of Master of Science in Engineering (Mechanical)
Department of Mechanical and Aeronautical Engineering

Western Michigan University
Kalamazoo, Michigan
December 2007

ACKNOWLEDGMENTS

I want to thank my advisor Dr. Parviz Merati for his great support and exceptional guidance throughout my graduate studies. In addition I would like to thank Dr. William Liou, Dr. Tianshu Liu for taking the time to review this thesis and serving as members of my committee.

I would also like to extend specific thanks to, Mr. Peter Thannhauser for his friendship, guidance and willingness to teach me the programming in LabView that have been used in numerous researches. Additionally, I would like to thank Mr. Glenn Hall for his training in machining, fabrication and extended discussions. These skills have proved invaluable in this and other research projects I have been involved in at Western Michigan University. Special thanks to my friends and fellow graduate students, Nathan J. Cooper Andrew O'Neill and Brandon Hulway for design advice and fabrication of this experimental setup.

Finally I would like to thank my family for their love and support throughout my entire college education years. I dedicated this work to my parents Wai Meng Leong and Kit Ngan Cheong, my brother Chin Tho Leong, and my sister An-Gie Leong.

Chin Hoong Leong

FLOW STRUCTURES IN AN ENCLOSED SIMPLIFIED FULL SCALE UNDER-HOOD ENGINE COMPARTMENT DURING STEADY STATE OPERATION

Chin Hoong Leong, M.S.E.

Western Michigan University, 2007

An experimental study of flow structures in an enclosed simplified full scale under-hood engine compartment will be conducted during steady state operation using whole field velocity measuring technique. 2D Particle Image Velocimetry (PIV) is planned for multiple cross sections in the test volume. Emphasis is given on understanding the flow structures of the 3D under-hood flow using multiple 2D PIV measurements. A recent study conducted on the engine compartment only consists of three 2D PIV measurement cross sections that sufficiently display 2D flow behavior at specific regions. Therefore, a detailed 3D flow mapping in the enclosure on various cross sections at different locations is conducted.

TABLE OF CONTENTS

ACKNOWLEDGMENTS ii

LIST OF TABLES v

LIST OF FIGURES vi

CHAPTER

I. INTRODUCTION 1

Scope of Project 2

II. EXPERIMENTAL SETUP 4

Enclosed Full Scale Simplified Under-Hood Compartment 4

Camera Traversing Base 12

Particle Image Velocimetry (PIV) 14

Thermal Measurements 15

III. MEASUREMENTS RESULTS 19

Temperature Measurements 19

Engine Block Surface Temperatures 19

Enclosure Surface Temperatures 22

Air Temperature 24

Particle Image Velocimetry Results 32

X-Y Planes Velocity Contours 32

Y-Z Planes Velocity Contours 38

Velocity Stream Traces 43

X-Y Planes Velocity Stream Tracers 44

Table of Contents—Continued

CHAPTER

Top Region 44

Left Region 47

Right Region 49

Bottom Region 50

Y-Z Planes Velocity Stream Tracers 52

Measurement Uncertainties 61

IV. CONCLUSION 62

BIBLIOGRAPHY 63

LIST OF TABLES

1. Thermocouple grid 16

2. Engine block surface temperature statistics 19

3. Engine block surface temperature statictics (no power to exhaust heaters) 22

LIST OF FIGURES

1. Measurement planes (a) X-Y planes, (b) Y-Z planes 3
2. Enclose full scale simplified under-hood compartment 5
3. Enclosed full scale simplified under-hood compartment overall dimensions 5
4. Layout of thermocouple access holes for air temperature measurement 6
5. Sealed chamber 7
6. Thermocouple routing in block shroud 8
7. Thermocouples in exhaust heater shroud 9
8. Exhaust heater assembly 9
9. Temperature control water circuit 11
10. Relay bank for computer control of temperature 12
11. Photograph of two-axis traversing platform 13
12. Engine block surface mesh for thermocouple measurements 16
13. Enclosure surface mesh for thermocouple measurements 17
14. Engine thermal cycle 18
15. Engine block surface temperature contours. 19
16. Engine block surface temperature (exhaust heaters not operated) 21
17. Enclosure surface temperature contours. 23
18. Response time calibration of the thermocouple for air temperature measurement 25
19. Locations for air temperature measurements. 26
20. Thermocouple insertion. 27

List of Figures—Continued

21. Response characteristics of the thermocouple 27

22. Thermocouple time constant from Omega 28

23. Thermocouple responses at several locations 28

24. Top row air temperature profile. 29

25. Second row air temperature profile 29

26. Third row air temperature profile 30

27. Fourth row air temperature profile 30

28. Bottom row air temperature profile 31

29. Columns 1 and 2 air temperature profile 31

30. X-Y plane at Z = 317mm with (a) Velocity magnitude contours, (b) Velocity standard deviation contours 33

31. X-Y plane at Z = 444mm with (a) Velocity magnitude contours, (b) Velocity standard deviation contours 34

32. X-Y plane at Z = 571mm with (a) Velocity magnitude contours, (b) Velocity standard deviation contours 35

33. X-Y plane at Z = 686mm with (a) Velocity magnitude contours, (b) Velocity standard deviation contours. 36

34. X-Y plane at Z = 736mm with (a) Velocity magnitude contours, (b) Velocity standard deviation contours. 37

35. Y-Z plane at X = 337mm with (a) Velocity magnitude contours, (b) Velocity standard deviation contours 39

36. Y-Z plane at X = 15mm with (a) Velocity magnitude contours, (b) Velocity standard deviation contours 40

37. Y-Z plane at X=236mm, 439mm, and 515mm with (a) Velocity magnitude contours, (b) Velocity standard deviation contours 41

List of Figures—Continued

38. Slant plane with (a) Velocity magnitude contours, (b) Velocity standard deviation contours 42

39. X-Y plane regions 43

40. Velocity stream tracers of top region in X-Y plane at Z = 317mm..... 45

41. Velocity stream tracers of top region in X-Y plane at Z = 444mm (middle location of the engine block) 45

42. Velocity stream tracers of top region in X-Y plane at Z = 571mm..... 46

43. Velocity stream tracers of top region in X-Y plane at Z = 686mm..... 46

44. Velocity stream tracers of top region in X-Y plane at Z = 736mm (front surface of engine block) 46

45. Velocity stream tracers of left regions in all X-Y planes 48

46. Velocity stream tracers of right regions in X-Y planes (a) Z=317mm, (b) Z=444mm 49

47. Velocity stream tracers of right regions in X-Y planes (c) Z=571mm, (d) Z=686mm, (e) Z=736mm..... 50

48. Velocity stream tracers of bottom regions in (a) Z = 317mm, (b) 444mm, (c) 517mm of X-Y planes 51

49. Velocity stream tracers of bottom regions in (d) Z = 686mm, (e) 736mm of X-Y planes..... 52

50. Location of Y-Z planes at X=236mm (C1), 337mm (C2), 439mm (C3), and 515mm (C4) 54

51. Velocity stream tracers of Y-Z plane at X = 337mm 55

52. Approximated 3-D vortices..... 55

53. Velocity stream tracers of partial Y-Z planes (a) X=236mm, (b) X=439mm, (c) X=515mm 56

54. Velocity stream tracers of Y-Z plane at X = 15mm (left side of enclosure) 57

List of Figures—Continued

55. Velocity stream tracers of Y-Z plane at X = 15mm with left glass outer surface temperature contours 58

56. Velocity stream tracers of 24mm away from right slant glass surface..... 59

57. Interpreted main flow structures (a) Top view, (b) Isometric view, (c) Front view, (d) Left side view..... 60

CHAPTER I

INTRODUCTION

Under-hood buoyancy flow has been a recent interest to the automotive industry as the struggle to minimize fuel consumption and improve automotive performance. Vehicle performance and fuel consumption are directly related to the gross weight of the fully assembled automobile. A wide range of light weight material such as plastic components, electronic sensors, and electrical wiring has raised concerns of possible meltdown during the absence of force convection cooling. Therefore, experimental study of the flow behavior in a natural convection under-hood buoyancy flow using a simplified model facilitates verification of computation fluid dynamics (CFD) models. CFD models would then allow low cost component placement design in a more complicated setup.

The objective of this thesis is to provide an understanding of the 3D flow structures using 2D PIV data during steady state operation. Measurements will be conducted in a full scale simplified under-hood configuration with a fully enclosed glass casing to allow for optical access. The simplified under-hood geometry that will be used for this study is the version from earlier General Motors R&D's under-hood model. Steady state operation simulates a certain time frame during an engine thermal "soak" condition. The vehicle is assumed to have undergone a high engine loading during an uphill load bearing climb. Shortly after, it is parked and shutdown in a windbreak environment allowing heat to built up in the under-hood compartment. Without force convection from the cooling fans and external air flow, heat from the engine components will dissipate and reticulate in the under-hood compartment. At the engine and exhaust temperature of 100 ^{o}C and 600 ^{o}C respectively is the steady state condition that the test setup simulates.

Recent studies by Merati[1] have provided 2D velocity cross sections of the simplified under-hood full scale model sufficiently display the flow behavior at 3 locations in a 2D manner using PIV. By scaling up from quarter scale model, fine details of additional vortices were found. The occurrence of these vortices was well defined in the measured 2D planes but in order to depict the third dimension of the flow further cross plane measurements have to obtain.

Scope of Project

The objective is to provide a better understanding of flow structures inside the simplified full scale under-hood model using PIV measurements. PIV measurements will be conducted on selected 2D cross sectional plane on X-Y and Y-Z planes. 2D data from Merati [1] were on the X-Y planes that showed buoyancy drive flow structures. Large vortices generated are suspected to move in and out of the X-Y plane and the cause of unsteady flow in certain areas is still unclear. More data are needed to determine the behavior of the dominant flow structures in a 3D sense. 2D velocity field from the planes shown in Figure 1 will provide a better understanding of these dominant flows in and out of the X-Y planes. Therefore, flow characteristics can be understood in a 3D sense.

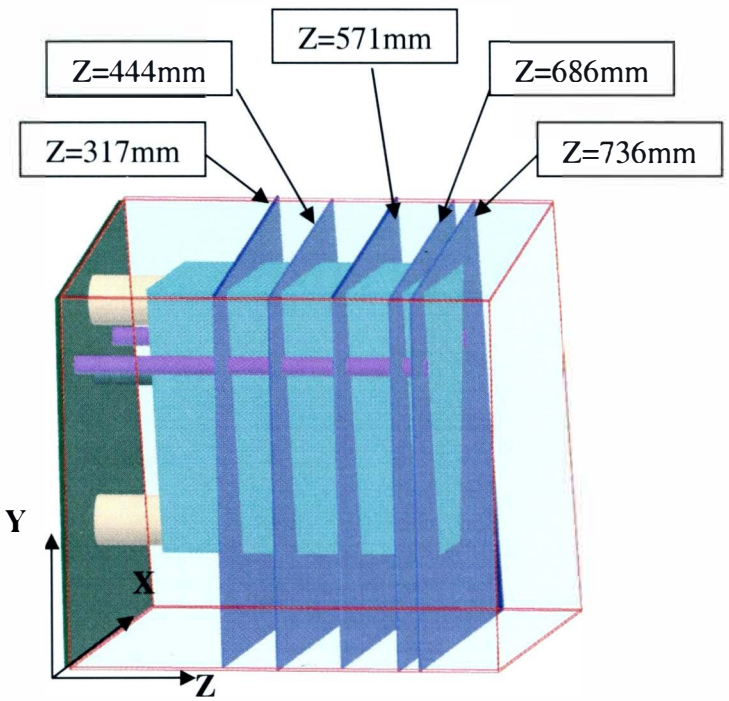

(a) X-Y Planes

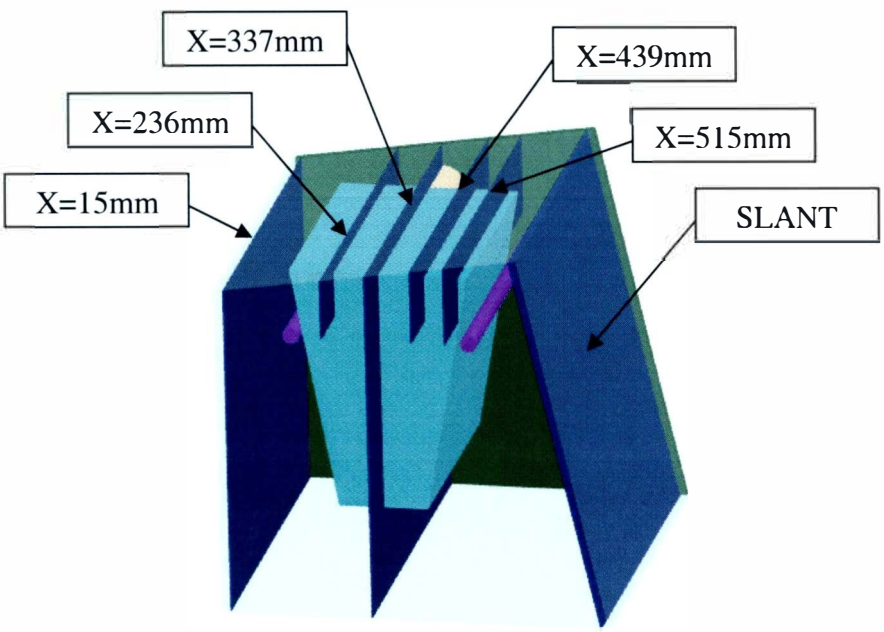

(b) Y-Z Planes

Figure 1. Measurement planes (a) X-Y planes, (b) Y-Z planes.

CHAPTER II

EXPERIMENTAL SETUP

Enclosed Full Scale Simplified Under-Hood Compartment

Flow field measurements will be conducted in a simplified full scale under-hood model shown in Figure 2 that have been used in previous study by Merati[1]. With specific surface temperature requirements, the engine block will be maintained at 100 ^{o}C, the cylinders which represents exhaust heaters will be at 600 ^{o}C, and temperatures on the glass enclosures have be measured during steady state operating condition and have been found to be repeatable. These surface temperatures will be monitored during operation to maintain required working temperature ensuring repeatability.

Fully enclosed glass case is used to ensure optical access for PIV measurements. The enclosure consists of the base, back wall, glass cover, calibration grid, and seeding mechanisms. The base is constructed of a 0.250" aluminum sheet with a window located directly below the engine block to allow illumination and observation for PIV measurement on the bottom surface of the block. The back wall is constructed of 0.500" aluminum sheet that provides structural surface for mounting the block and exhaust heaters. The back wall also contains holes patterns that provide access for air temperature measurements. The layout of these holes is shown in Figure 4. The glass cover seals the underhood environment while allowing visual observation and illumination for PIV measurements. The calibration grid is a 0.125" sheet aluminum cut out to fit around the block and exhaust heaters. The grid is mounted to two rods that allows it to be moved forward to the plane of interest. An image is captured from the grid before any PIV measurements are made to allow for scaling of the image and stitching of many images into a composite velocity profile. The seeding consists of injection through a small tube

the image and stitching of many images into a composite velocity profile. The seeding consists of injection through a small tube in the back wall.

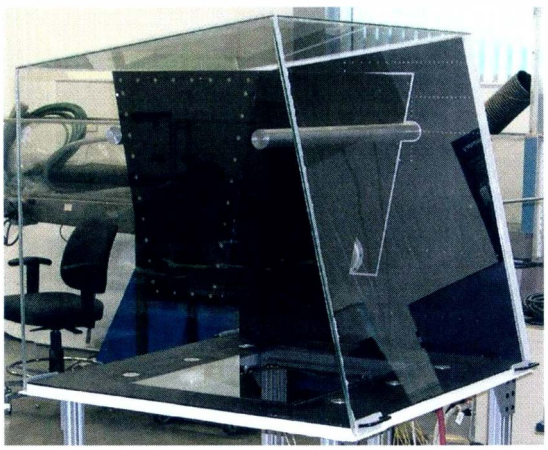

Figure 2. Enclose full scale simplified under-hood compartment.

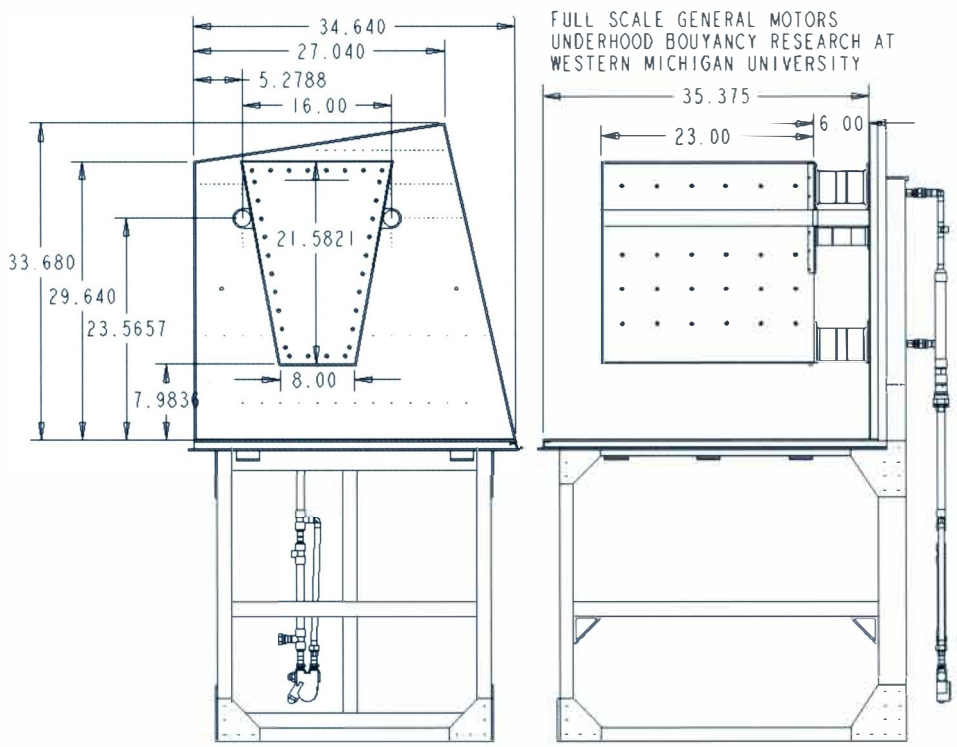

Figure 3. Enclosed full scale simplified under-hood compartment overall dimensions.

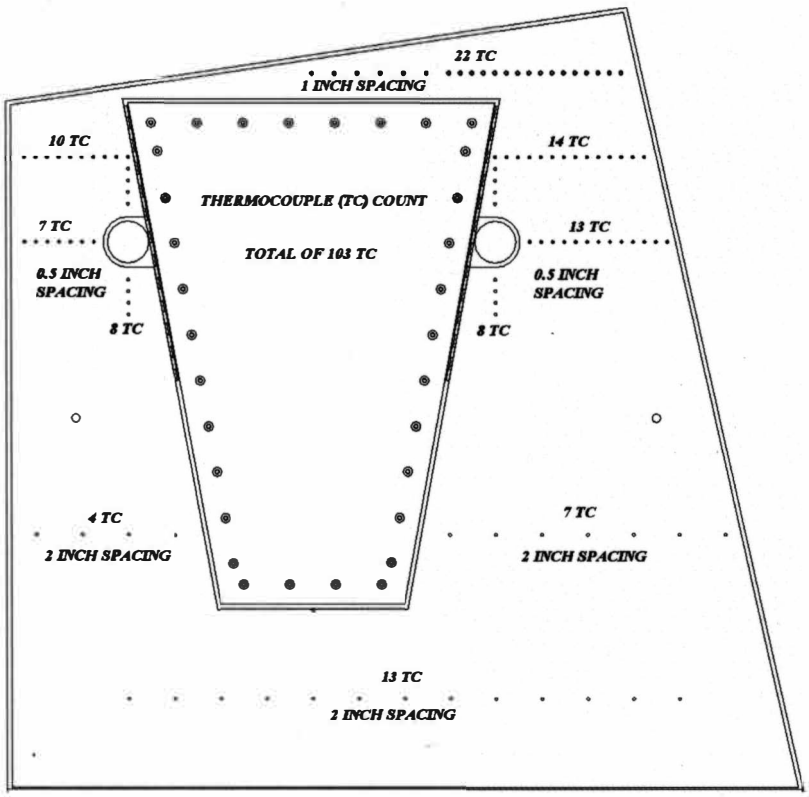

Figure 4. Layout of thermocouple access holes for air temperature measurement.

The block, representing the engine block, oil pan, engine heads, and intake manifold, consists of a sealed chamber for holding the water that maintains the temperature of the block, and a shroud that locates and hides the thermocouples used to map temperature profiles along the block. The sealed chamber is constructed of 0.250" aluminum plate and an aluminum frame. A spray manifold is located inside the sealed chamber to maintain a constant film of water on all the inner walls of the sealed chamber. An immersion heater is placed inside the sealed chamber for heating of the water and block. Photographs were obtained during a test where the top and front walls were Plexiglas to observe the spray pattern and validate coverage of all surfaces with water. Figure 5 shows this setup with the spray manifold, immersion heater, and return line for the water circulation system.

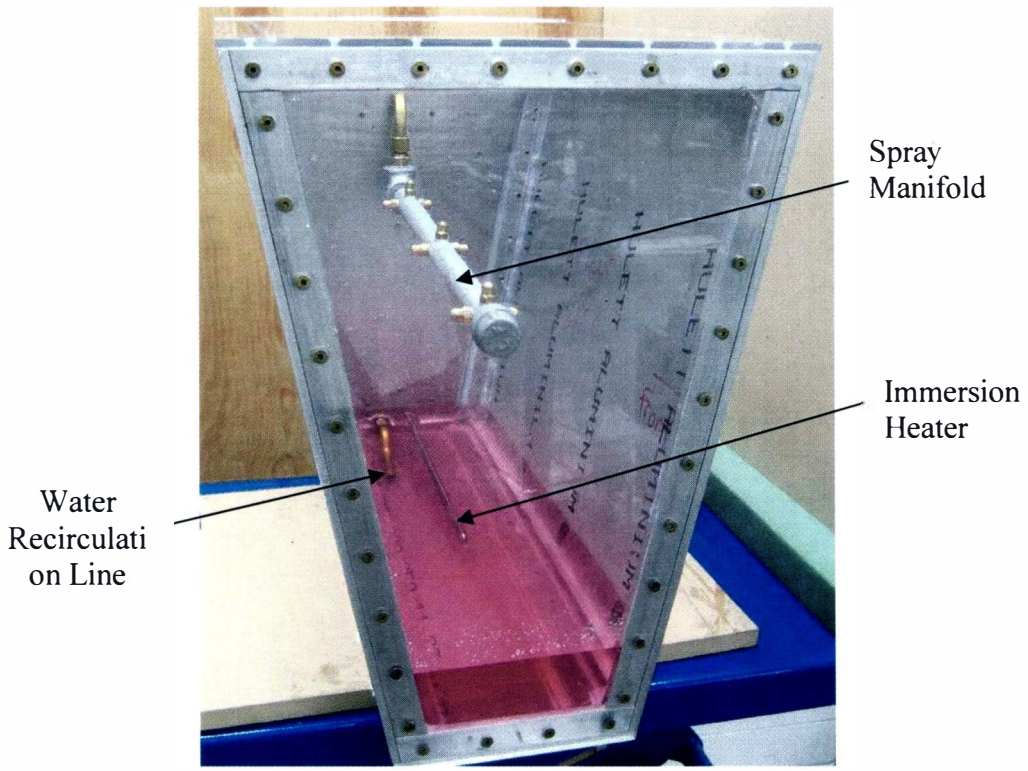

Figure 5. Sealed chamber.

The shroud was constructed of 0.250" aluminum plate on the back and 0.125" aluminum plate on the sides, top, and bottom. The shroud allows for thermocouples to be located at many points on the block without disturbing airflow, which will allow for validation of consistency from one run to the next. The thermocouples are placed in groves machined into the shroud plates as shown in Figure 6. The majority of thermocouples are located on the sides near the exhaust heaters as this is where the largest temperature gradients are expected. The shroud is attached to the sealed chamber through the use of #4 flat head screws in a grid.

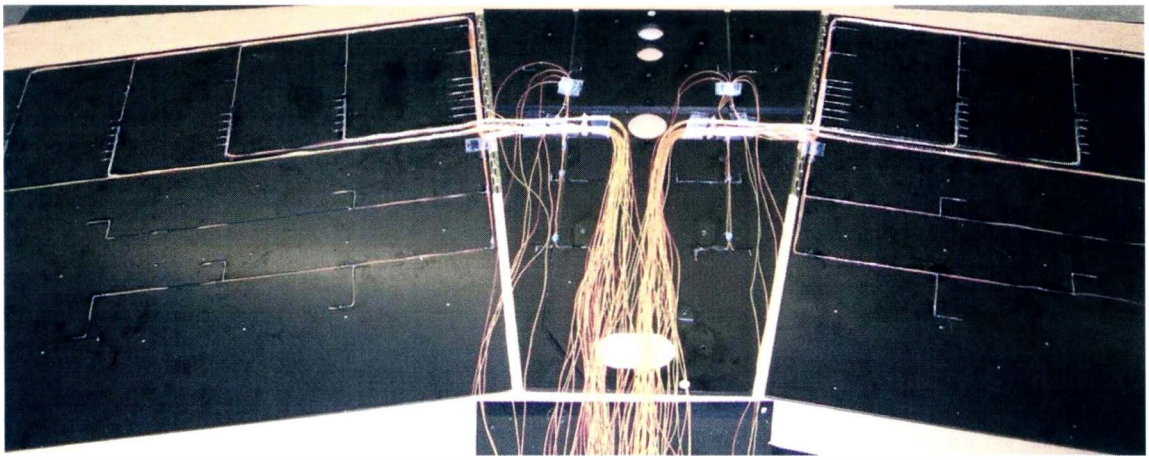

Figure 6. Thermocouple routing in block shroud.

The block assembly is attached to the back wall with three stainless steel standoffs. These standoffs are constructed from standard pipe and fittings, with the top and bottom providing support as well as feed-through for circulating water and power wires for the immersion heaters.

The exhaust heaters, representing the exhaust manifold, consist of a cartridge heater, a steel shroud, a ceramic insulator, and a standoff. The cartridge heater is custom made with a 3,500 Watt power rating, 22" heated length and a 0.750" diameter. There is a 0.375" long cold section on the end, which was required for manufacturing, and a 3" long cold section where the wires extend to protect the power leads.

The shroud was constructed from mild steel. Two halves were machined to have a compression fit on the cartridge heater and grooves for six thermocouples 0.1" from the outer surface. These thermocouples are located on a horizontal plane in pairs on opposite sides at 11.5", 15.5", and 16.5" from the base of the 23" long steel shroud. The two halves were joined using bolts, and a band of steel on the end closest to the back wall as the thermocouples prevented the use of a bolt. Once assembled, the bolts were welded over and the whole assembly was then turned on a lathe to the final dimensions. A 0.500" thick ceramic spacer was machined to insulate the exhaust heater from the

stainless standoff. The standoff is constructed from stainless pipe with the outer diameter machined to match that of the exhaust heater and ceramic insulator. The thermocouple locations and the completed exhaust heater assembly can be seen in Figures 7 and 8, respectively.

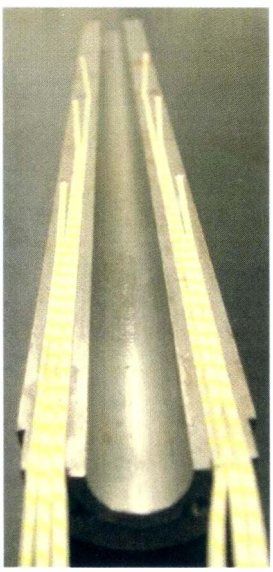

Figure 7. Thermocouples in exhaust heater shroud.

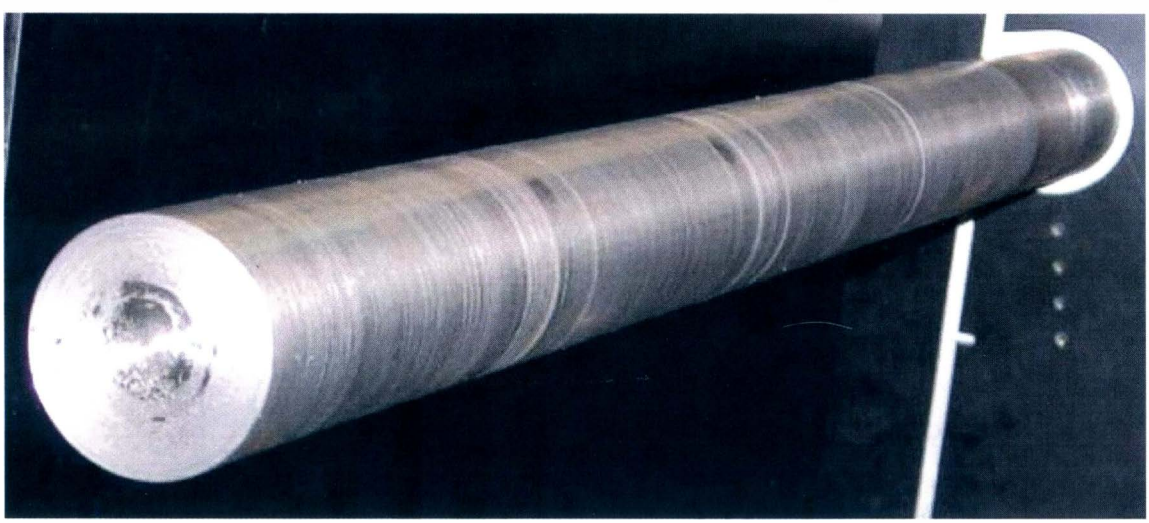

Figure 8. Exhaust heater assembly.

The control of temperature for the simulated underhood environment required a water circulation loop and a relay bank control of power. The water circulation loop shown in Figure 9 consists of a return line that runs from the sealed chamber of the block through the regenerative heat exchanger, through the cooling heat exchanger, and to the pump. The pump chosen is a rotary vane pump that allows for high pressure with low flow rates. The heat exchangers are required to cool the water before it reaches the pump to prevent cavitation. The water leaves the pump through the return line, passes through the regenerative heat exchanger and then passes an inline immersion heater before returning to the sealed chamber through the spray manifold. The regenerative heat exchanger and the inline heater reheat the circulated water so that the overall temperature of the block can be maintained. The relay bank consists of four relays that are controlled by the data acquisition system. Two are used to control the power to the two exhaust heaters, one is used to control power to the immersion heater in the sealed chamber, and the last one switches the power to the circulation pump on and off. This relay bank is housed in an aluminum box as shown in Figure 10.

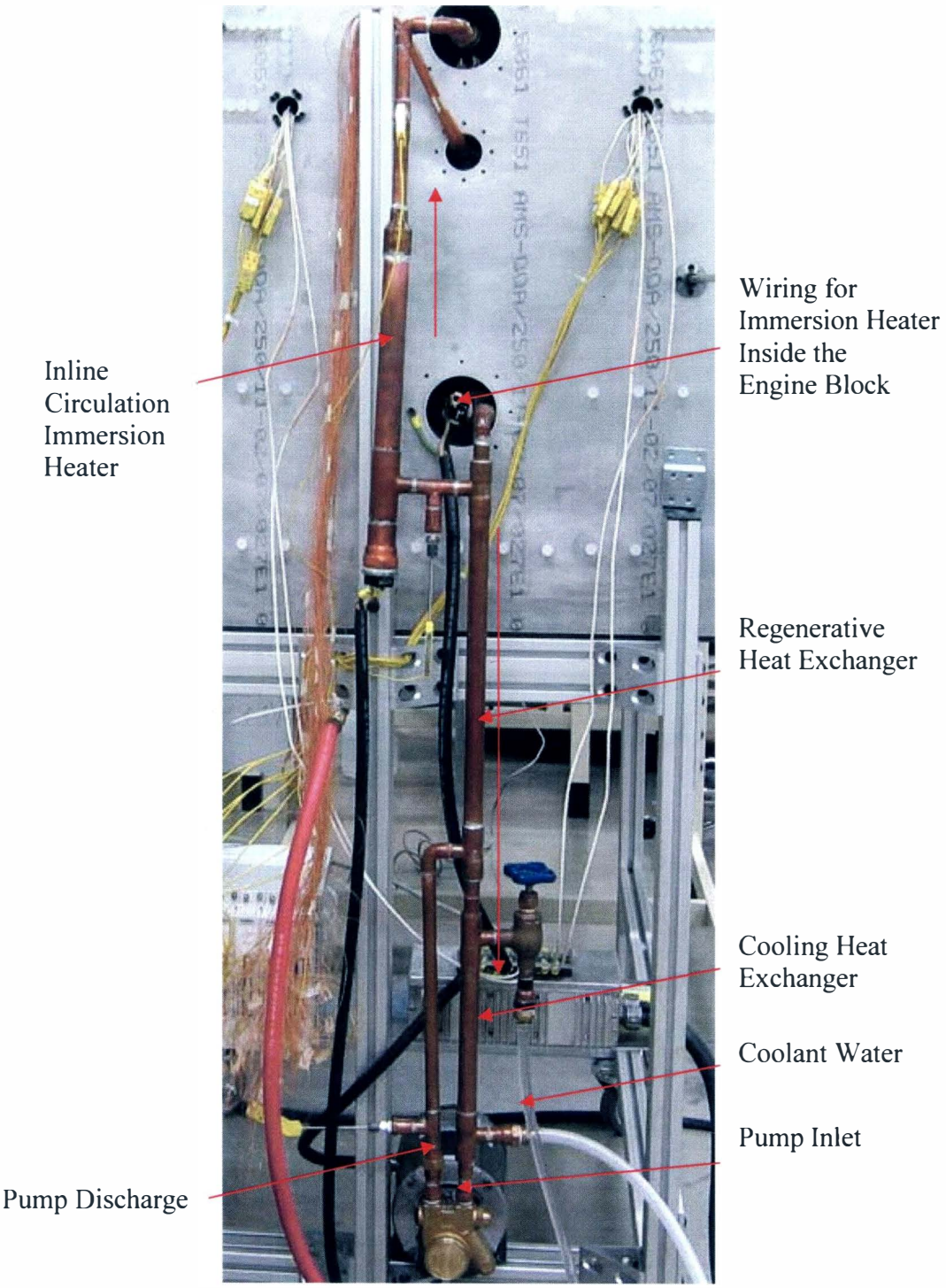

Figure 9. Temperature control water circuit.

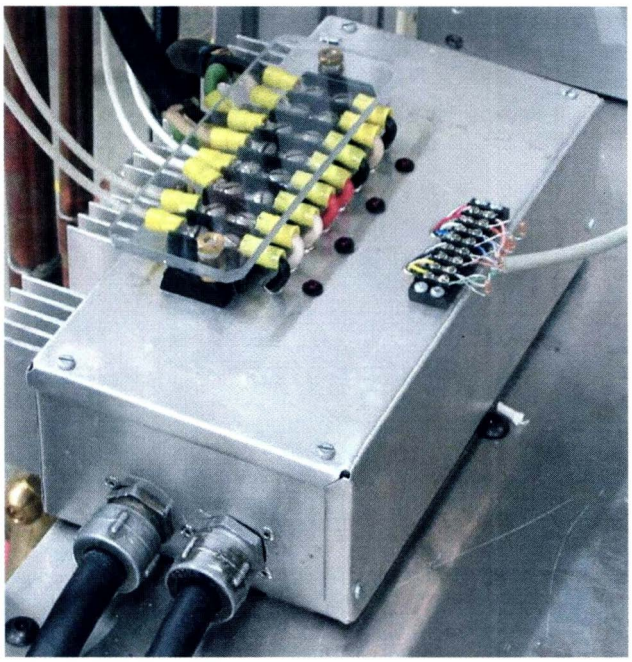

Figure 10. Relay bank for computer control of temperature.

The control of temperature in the simulated engine compartment focuses on maintaining the surface temperature of the block and of the two exhaust heaters. The control of exhaust heater surface temperature relies on a feedback control loop written into the LabView software, and the surface temperature of the block is controlled through the use of the heat pipe concept. The heat pipe allows for control of surface temperature without a control loop, and the use of embedded cartridge heaters in the exhaust heaters allows for the 600 °C.

Camera Traversing Base

For increase accuracy and reduce equipment setup time, a two-axis traversing platform for the digital camera was developed. Shown in Figure 11 a PIV camera is mounted on a holder that allows for fine tilt, pan, and rotation adjustments. The camera holder is mounted on to the Y-axis base for vertical motion translation which is then mounted on an X-axis base that allows horizontal motion. A digital control systems

and program were also developed to accurately traverse the camera in both directions accurately. Using a quadrature encoder on each motor as position sensor coordinates can be input into the program to locate the camera without the need of a calibration grid. This speeds up data acquisition process as the program can be calibrated for set locations before experiments eliminating the frequent use of a retractable calibration grid. These coordinates will then be used in stitching multiple regions.

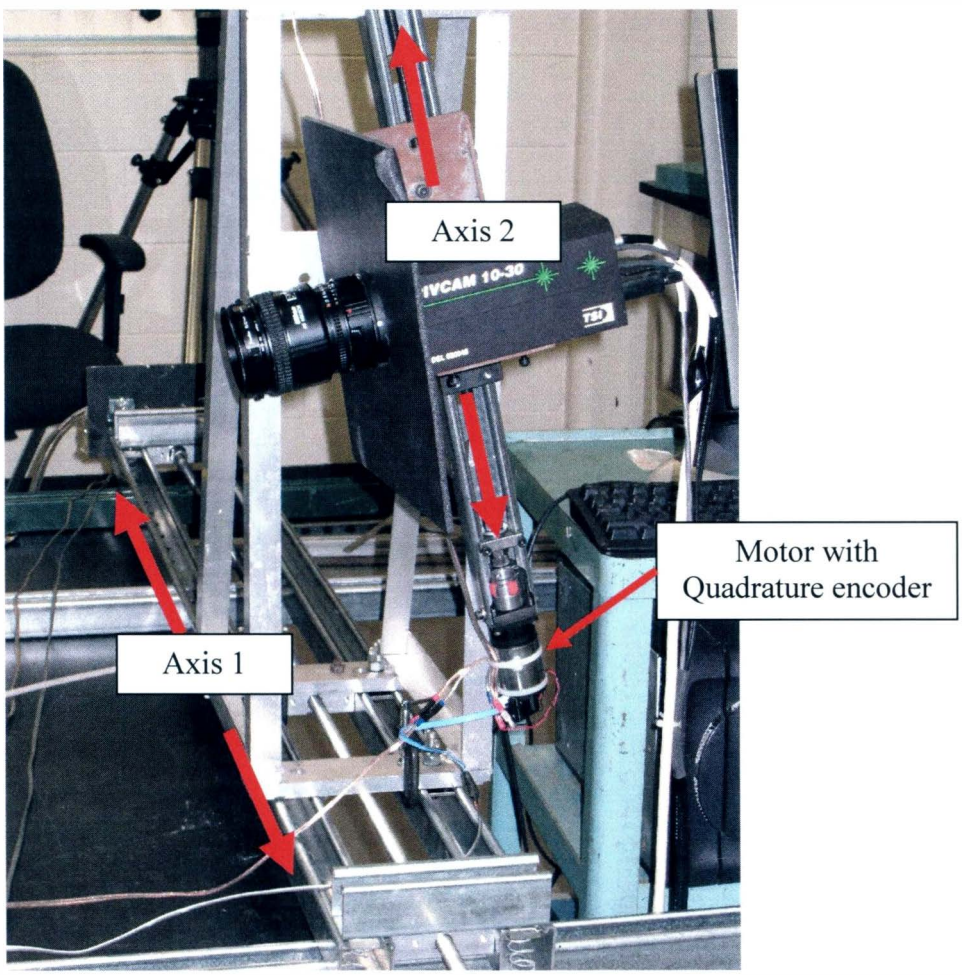

Figure 11. Photograph of two-axis traversing platform.

Particle Image Velocimetry (PIV)

Particle Image Velocimetry (PIV) is a non-intrusive measurement technique for retrieving two and three dimensional velocity information from fluid flows. For this experiment, a 2D PIV system is used. This technique requires two laser sheets firing at different time, a camera located perpendicular to the laser sheet that is capable of capturing the light reflected from the lasers, and seeding particles that will track the fluid flow movements. Since the camera has a limited view area of 7 centimeters by 7 centimeters, multiple regions in a cross sectional plane will be captured and will need to be combined to produce flow field for a full plane. Multiple planes will be obtained to produce sufficient information for a 3D flow field analysis.

The flow field in the measurements domain contains high temperature air. Therefore, chalk particle sizes of 3 to 30 microns and a specific gravity of 2.06 will be used as tracer to prevent combustion. A 190 mJ Nd:YAG PIV laser system manufactured by Big Sky Laser was used in the project. A PIVCAM 10-30 digital camera Model 630046 distributed by TSI with a resolution of 1000(H) x 1016(V) pixels at 8-bits was used. The firing of the laser is synchronized with the camera using a synchronizer Model 610032 and a PIV software package called Insight v5.0 developed by TSI. The software package records and processes images captured for velocity information extraction. For each image pair, a FFT algorithm from the software is used in conjunction with automatic vector validation to remove erroneous vectors. Interrogation areas of 64 x 64 pixels (~5mm x 5mm) were set for faster processing due to the size of each measurement planes. These regions were then combined using programs developed in the Fluids Mechanics Laboratory producing a unified measurement plane for better understanding.

Thermal Measurements

Each engine block surface, except front surface, is embedded with thermocouples. External thermocouples are attached to the engine block front surface and enclosure surfaces. The temperature measurements are taken by four-32 channel temperature data conditioning modules and a National Instrument data acquisition card. Furthermore, these measurements are monitored and recorded by a LabView code developed at WMU. The results are then converted to the Tecplot format (FE Block, cell-centered). The thermocouple mesh size and associated areas for each of the engine block and enclosure surfaces are shown in Table 1. The temperature measurement mesh for the engine block and the enclosure surfaces are presented in Figures 12, and 13, respectively. The temperature values are obtained at the center of the cells. The temperature of the twelve thermocouples embedded in the two exhaust heater shrouds and the three thermocouples in the water circulation loop are monitored to assure that the system has reached steady state condition. Three water circulation loop thermocouples are located before and after the inline immersion heaters on the return line, and on the pump discharge.

	Location, Side (s)	Thermocouple Grid	Average TC Cell Area (cm²)
Engine Block	Front (I)	4 × 9	48.1
	Back (II)	4 × 3	150.3
	Right (III)	5 × 11	82.9
	Left (IV)	5 × 11	82.9
	Top (V)	2 × 3	390.3
	Bottom (VI)	2 × 3	196.9
Glass Enclosure	Front (VII)	7 × 9	102.7
	Right (VIII)	9 × 11	123.6
	Left (IX)	9 × 11	107.3
	Top (X)	9 × 11	99.4
	Back (XI)	7 × 9	102.7
	Bottom (XII)	4 × 7	283.3

Table 1: Thermocouple grid.

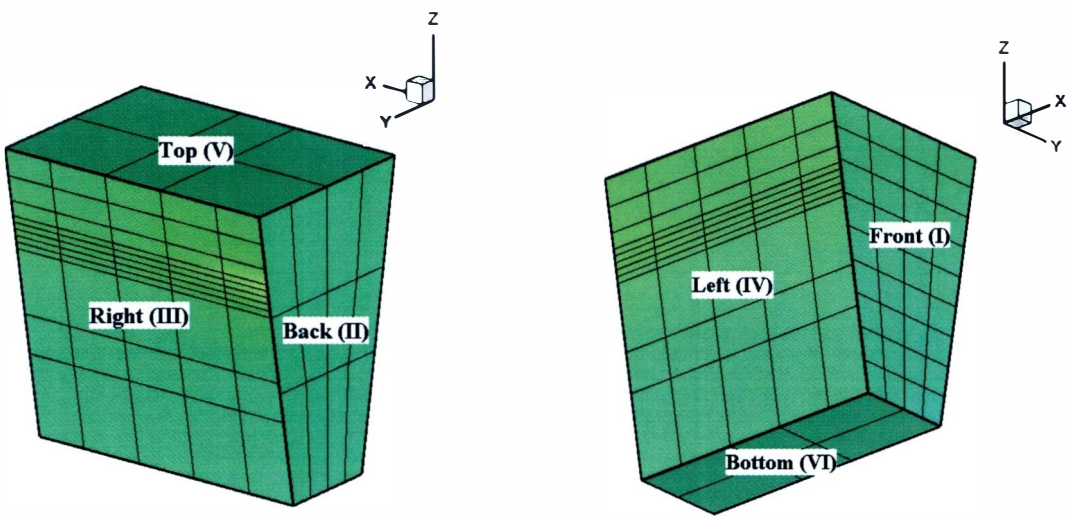

Figure 12. Engine block surface mesh for thermocouple measurements.

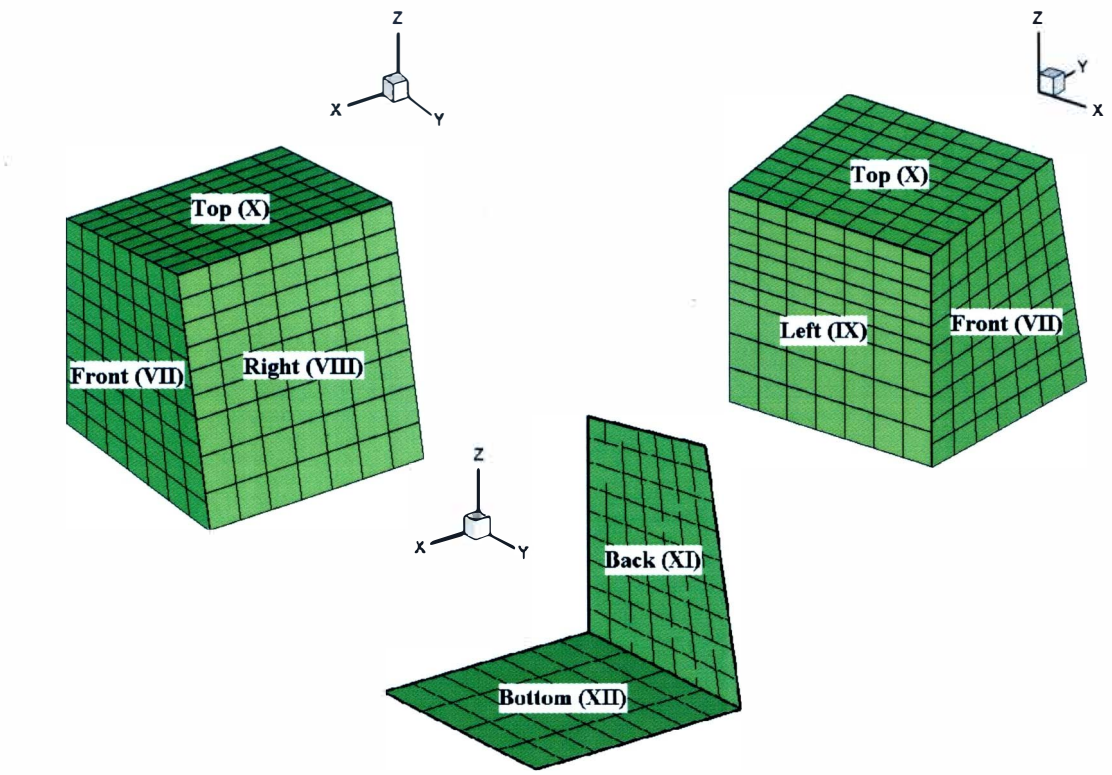

Figure 13. Enclosure surface mesh for thermocouple measurements.

The engine block is heated internally by water near saturation and externally by the exhaust heaters. The enclosure and the space within the enclosure are heated by the engine block and exhaust heaters. The exhaust heaters are heated to 600 °C, and water spray temperature inside the block is kept at 95 °C. The exhaust heaters, water temperature inside the block, and the average block surface temperature reach their desired steady state temperature after 3,600 sec as shown in Figure 14. All tests are then conducted at this steady state condition.

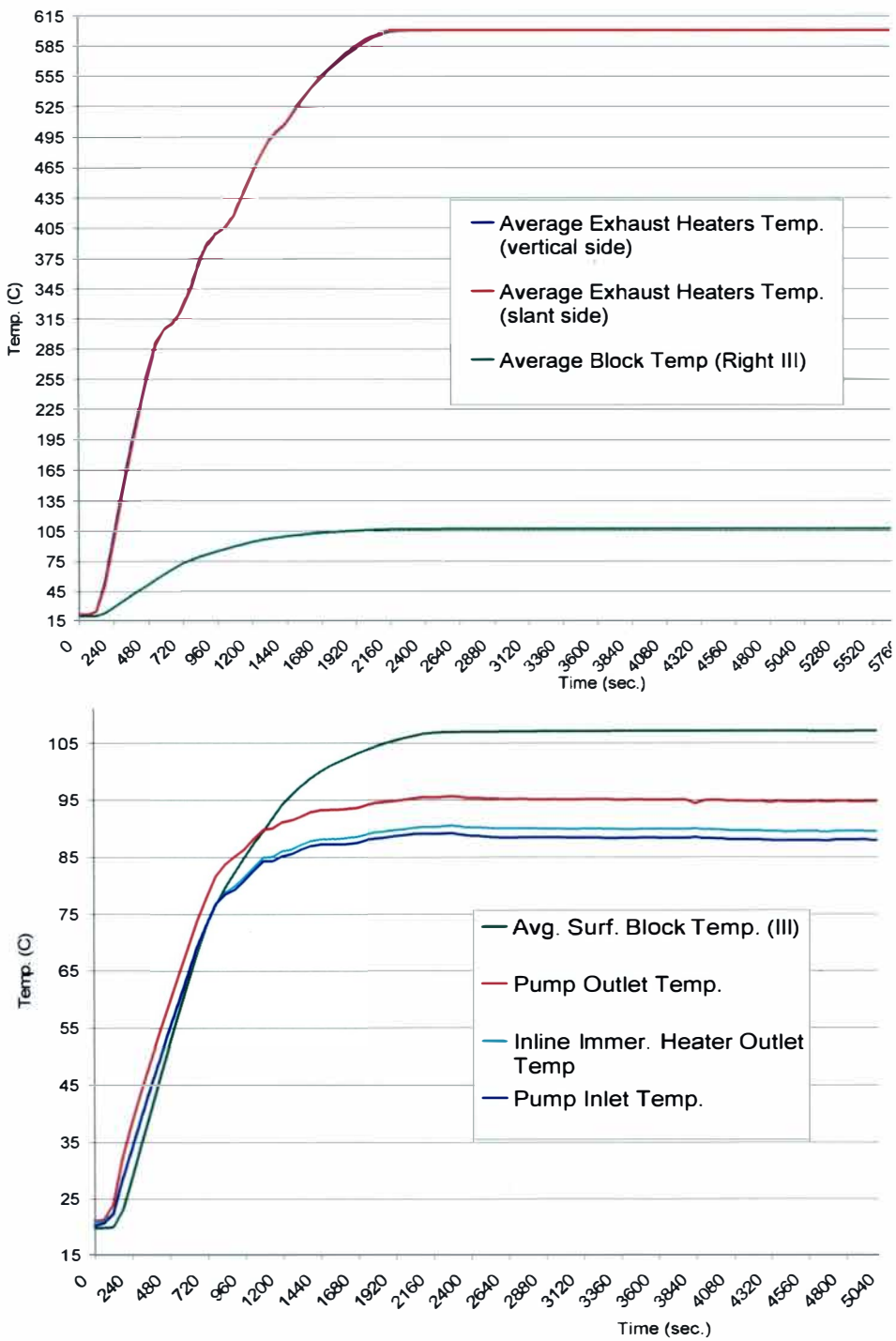

Figure 14. Engine thermal cycle.

CHAPTER III

MEASUREMENTS RESULTS

Temperature Measurements

Engine Block Surface Temperatures

The temperature contours for the top (V), bottom (VI), right (III), left (IV), back (II), and front (I) faces of the engine block are presented in Figure 15 and the corresponding statistics are presented in Table 2.

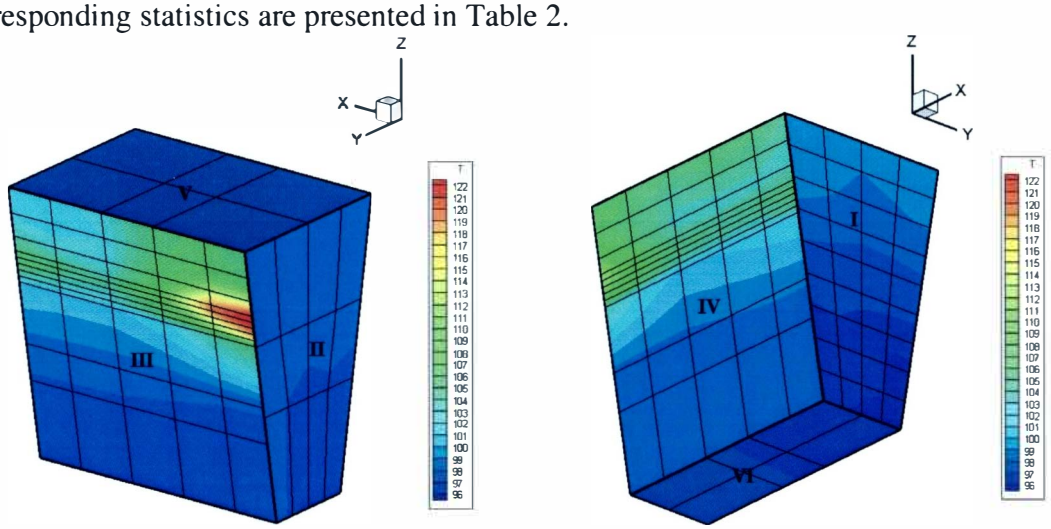

Figure 15. Engine block surface temperature contours.

Engine Block Surface Temperature C°						
	Front (I)	**Back (II)**	**Right (III)**	**Left (IV)**	**Top (V)**	**Bottom (VI)**
Mean	97.6	98.2	105.1	103.8	98.6	97.9
Std Dev	1.4	0.5	7.0	4.2	0.1	0.5
Max	99.7	98.9	123.2	113.6	98.8	98.2
Min	94.3	97.2	97.6	98.2	98.4	97.1
Range	5.3	1.7	25.6	15.4	0.4	1.2

Table 2: Engine block surface temperature statistics.

The discontinuity of the temperature magnitudes at some of the corners, especially between the right (III) and back (II) faces is due to the large mesh size for the temperature measurements. The thermal contours presented assume constant temperature over a cell area and does not take into account its thermal gradient. This is because temperatures were only obtained at the center of cells. Measurements of thermal gradients over the cells require extensive time and effort.

There are small temperature gradients at the front (I), back (II), top (V), and bottom (VI) surfaces as shown in Figure 15 and Table 2. The temperature is slightly higher at the top corners and becomes lower as the distance of Z-axis decreases for the front face. The highest temperature value is found at the right (III) surface closest to the exhaust heater. At the right (III) and left (IV) surfaces, the temperature is high along the axis of the exhaust heaters and becomes lower as the distance from the heaters increases. In addition, the temperature is lower at the bottom of each surface. Temperature gradients exist along the X-axis at the right (III) and left (IV) surfaces.

In the upper back corner of the left and right faces, the temperature is high near the back face, more noticeable on the right (III) surface. In order to verify that this is a real effect and not due to the design of the engine heating system, the engine block was heated to the desired temperature without turning on the heaters for the exhausts. Under this condition, a uniform surface temperature for the engine block is expected. Any deviation from this is most likely due to the errors caused by the thermocouple measurements and the engine block heating system. As observed by temperature contours shown in Figure 16 and temperature statistics presented in Table 3, the surface temperature gradients are much smaller than what were observed with the exhaust heaters at 600 °C. Thus, the observed thermal behavior of the engine block surfaces is caused by radiated and connected heat from the exhausts and not due to the experimental errors.

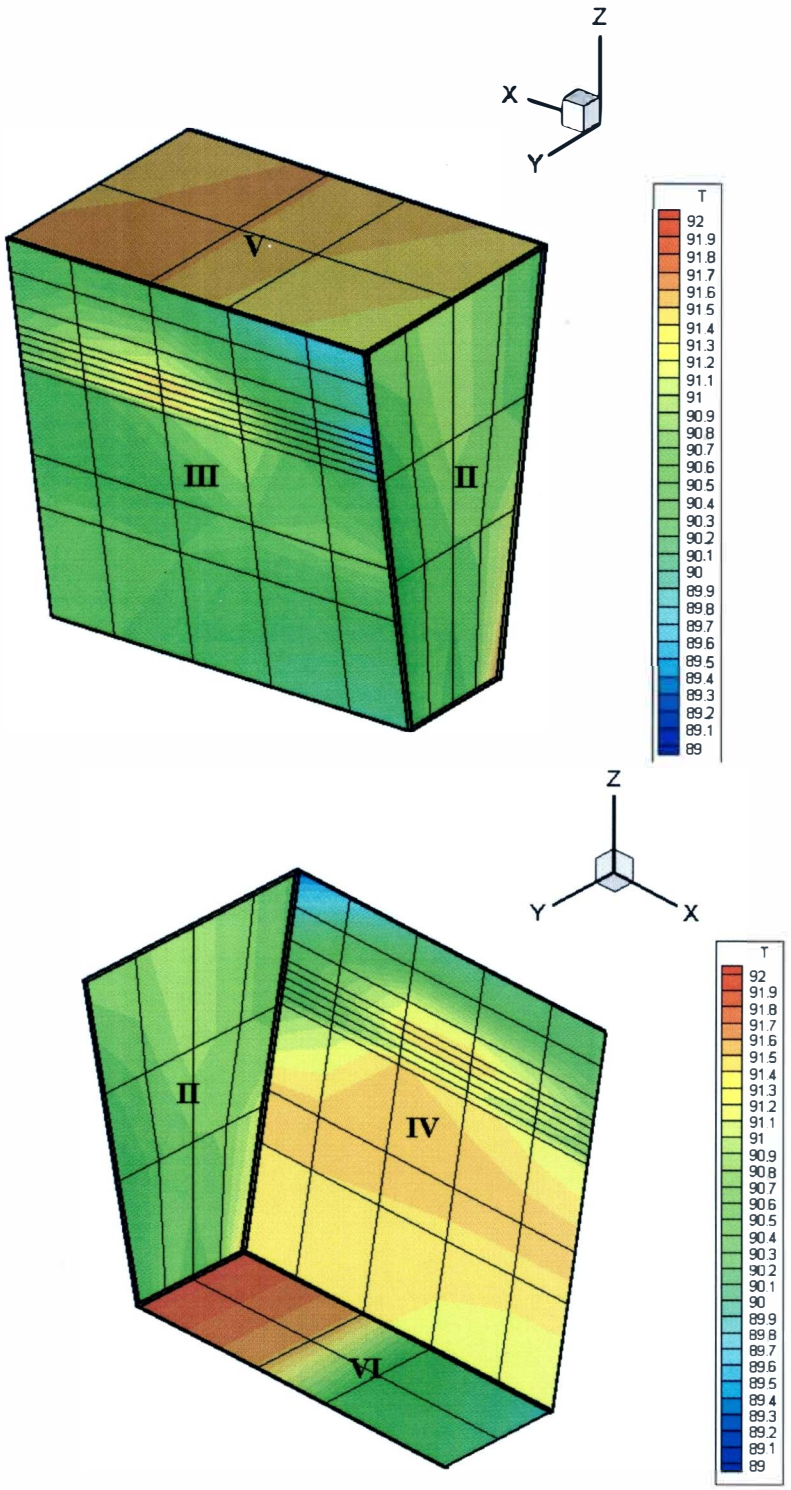

Figure 16. Engine block surface temperature (exhaust heaters not operated).

Engine Block Surface Temperature °C					
	Back (II)	Right (III)	Left (IV)	Top (V)	Bottom (VI)
Mean	89.7	89.1	89.3	89.6	90.6
Std Dev	0.3	0.3	0.2	0.2	0.6
Max	90.4	89.8	89.6	89.8	91.0
Min	89.3	88.2	88.6	89.4	89.4
Range	1.1	1.5	1.0	0.4	1.6

Table 3: Engine block surface temperature statistics (no power to exhaust heaters).

Enclosure Surface Temperatures

The temperature magnitudes are measured on the outside surfaces to prevent the thermocouple wires from disturbing the flow inside the enclosure. The temperatures on the back (XI) and bottom (XII) faces had to be measured on the inside because of the design constraints. The enclosure surface temperature contours are shown in Figure 17.

The high temperature regions are located directly above the exhaust heaters on the top face and closest to the exhaust heaters on the right (VIII) and left (IX) faces. The high temperature of these regions is mostly caused by radiation from the exhaust heaters as described in the following section. Temperature distributions on the front surface (VII) show similar characteristics as the engine block front surface. The temperature is highest at the top two corners with thermal gradients along the Y and Z axes. The back face is warmer than the bottom surface with an obvious rise in temperature approaching the exhaust heaters.

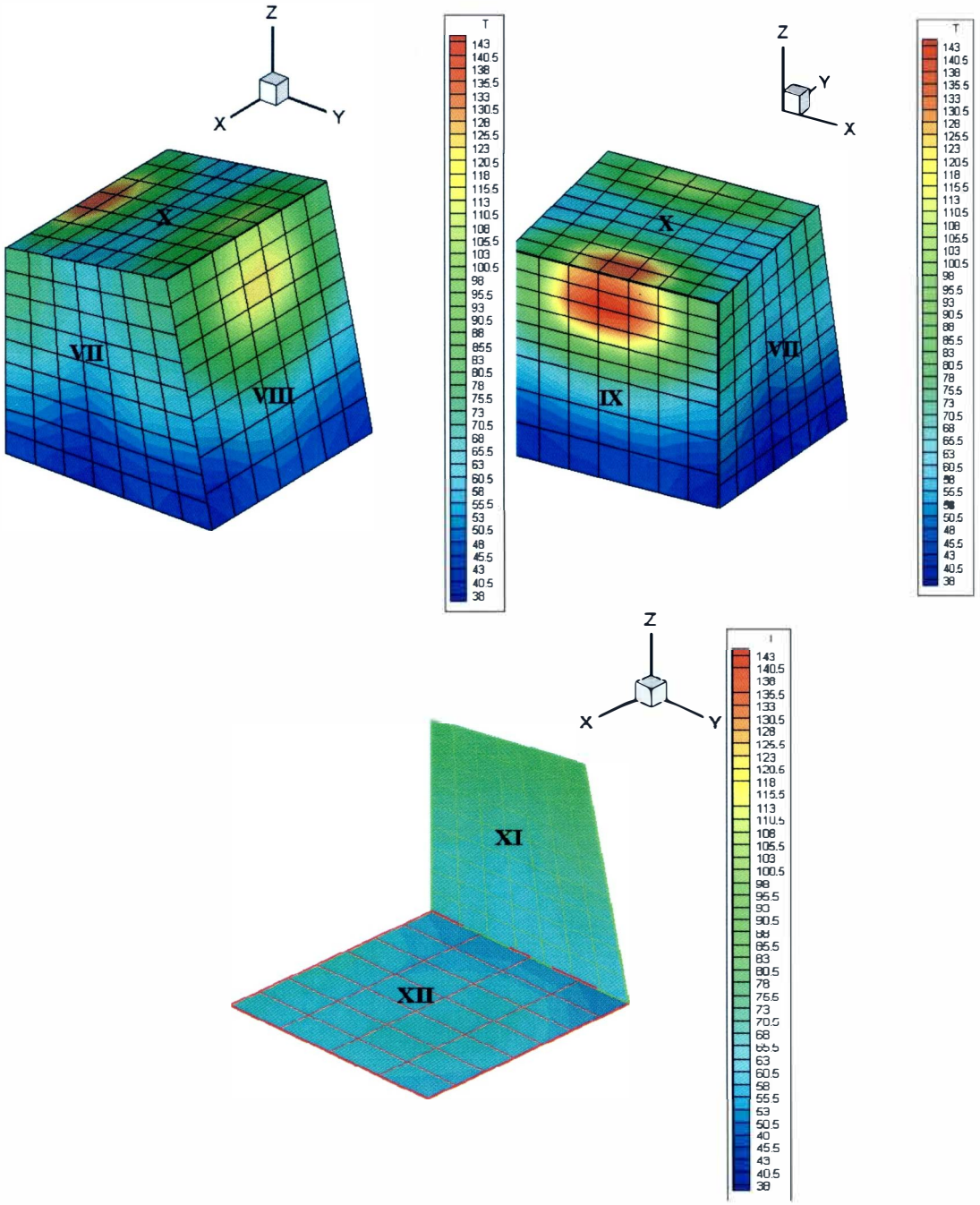

Figure 17. Enclosure surface temperature contours.

Air Temperature

Air temperature measurements are obtained on the middle plane with the location labeled in 19. These locations are scaled up from the quarter scale model and the number of the locations has been increased to over 4 times with a total of 104 locations. Since active flow structures in the quarter scale are concentrated in the upper portion of the enclosure, most of the temperature measurements were conducted here. Due to structural integrity of the back plate as part of the support for the engine block, extensive access holes were not implemented.

First, the thermocouple used for air temperature measurements was calibrated for response time with the setup shown in Figure 18. Hot air is being supplied by a heat gun and the air temperature inside the copper piping is being measured by Thermocouple B. Before a steady state temperature can be reached, Thermocouple A is kept within the fitting (in black). Once temperature reaches steady state, Thermocouple A is moved into the middle of the hot air stream to measure its response shown temperature in Figure 21. The motion of insertion of thermocouple A caused a 'bump' in the response curve even after multiple repetitions. Since radiation in the calibration setup is at a minimal, Thermocouple A would reach an almost constant temperature after 5 sec of exposure. Temperature of Thermocouple B decreases slightly after insertion of Thermocouple A due to air flow blockage. The difference in temperature obtained by the two thermocouples is possibly due to differences in thermocouple type, which is butt welded bare wire for TC A as to a stainless steal grounded thermocouple.

According to information given by product manufacturer, Omega, it is confirmed from Figure 22 with a diameter of 0.035 inches on the butt wield it requires 2 sec x 1.5 (for butt wield) which give a final value of 3.5 sec to respond to a 63.2 percent of temperature measurements. Using linear extrapolation, it will require about 5 seconds for

full temperature so a 5 seconds cut off for actual air temperature will be acceptable. Data are recorded for at least 45 seconds with some examples shown in Figure 23. The data shows a general slow increase in temperature since the thermocouple is exposed to not only hot fluid but also radiation from the heated cylinders. Therefore, a cut off time is required.

Figure 24 to 29 show the results of the air temperature starting from top to bottom row. Air temperature on the left side is consistently higher then the right side. The temperature profile for the first row show the presence of the hot plume and the lobes on the side are consistent with the mixing occurring due to the secondary flows observed by the PIV measurements. Air temperatures from column 2 are higher then in column 1 which is an indication of a hotter thermal layer around the right exhaust heater and the upper right engine block surface. This can only be verified with extensive thermal boundary layer measurements with accurate traversing thermocouple measurements to resolve the large temperature gradients in these regions.

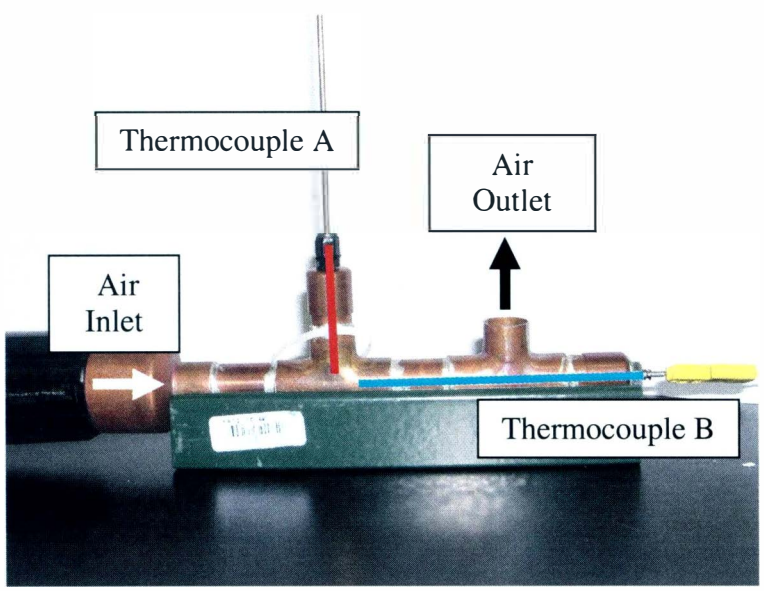

Figure 18. Response time calibration of the thermocouple for air temperature measurement.

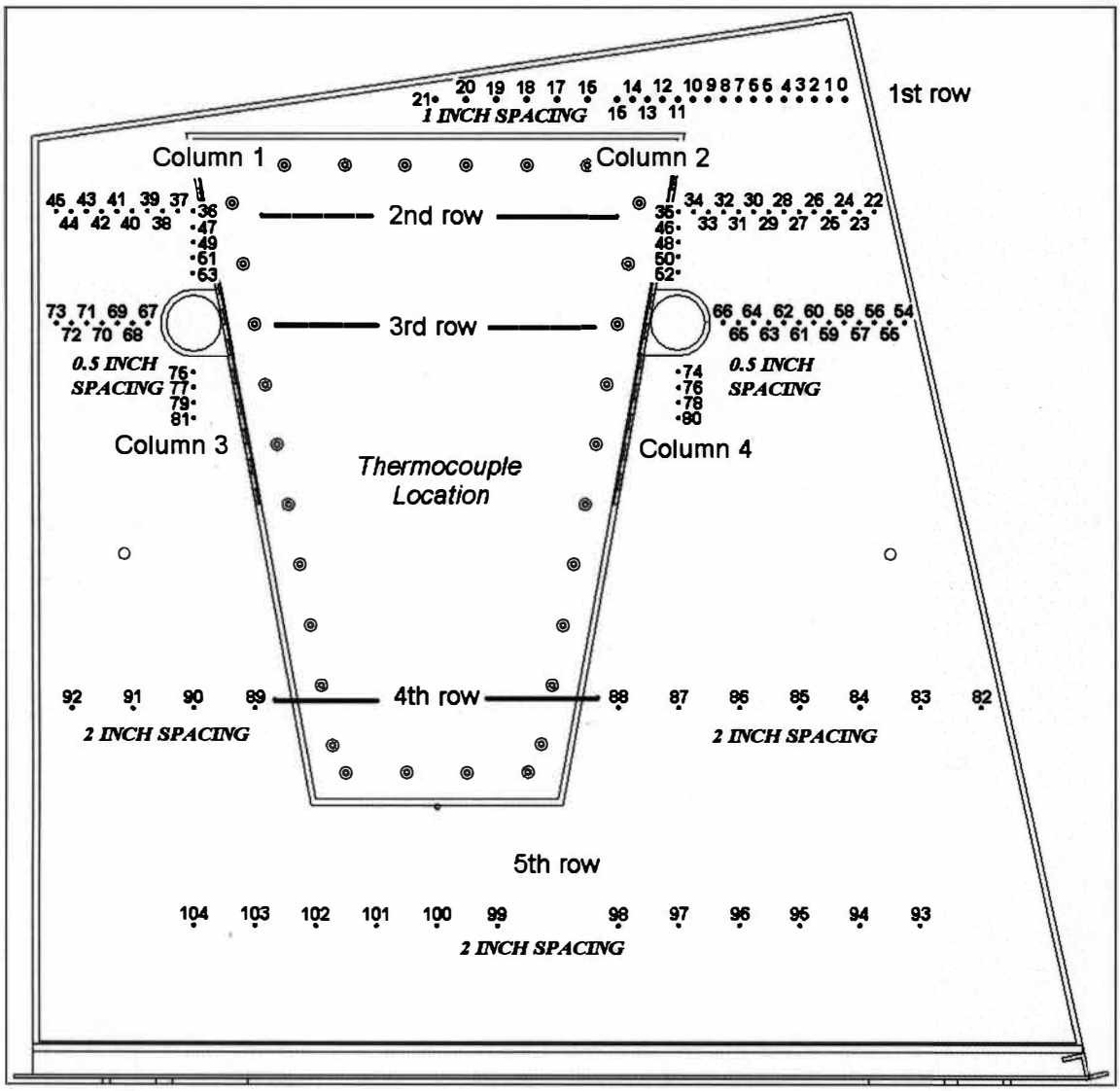

Figure 19. Locations for air temperature measurements.

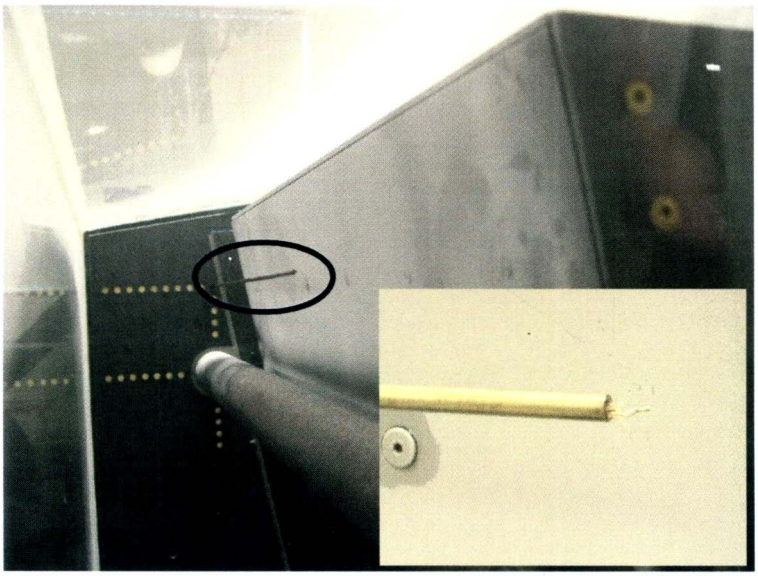

Figure 20. Thermocouple insertion.

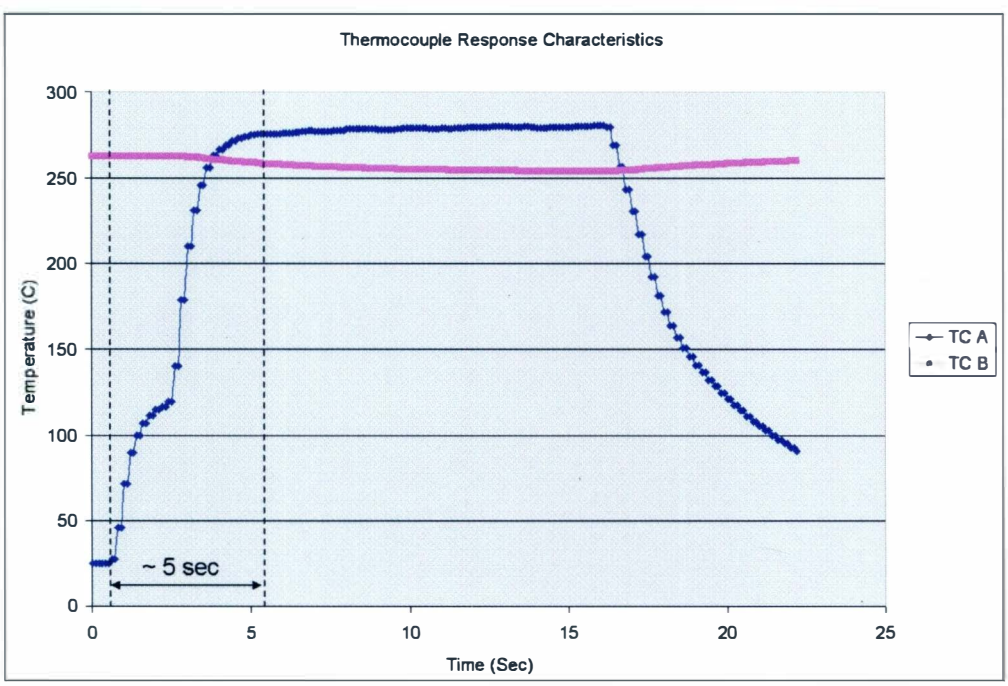

Figure 21. Response characteristics of the thermocouple.

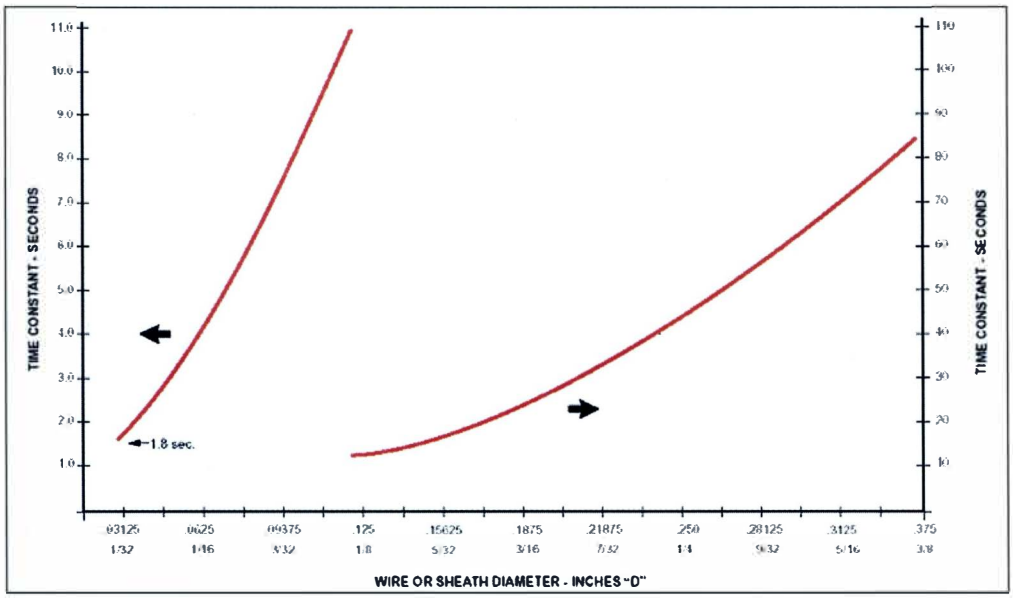

Figure 22. Thermocouple time constant from Omega.

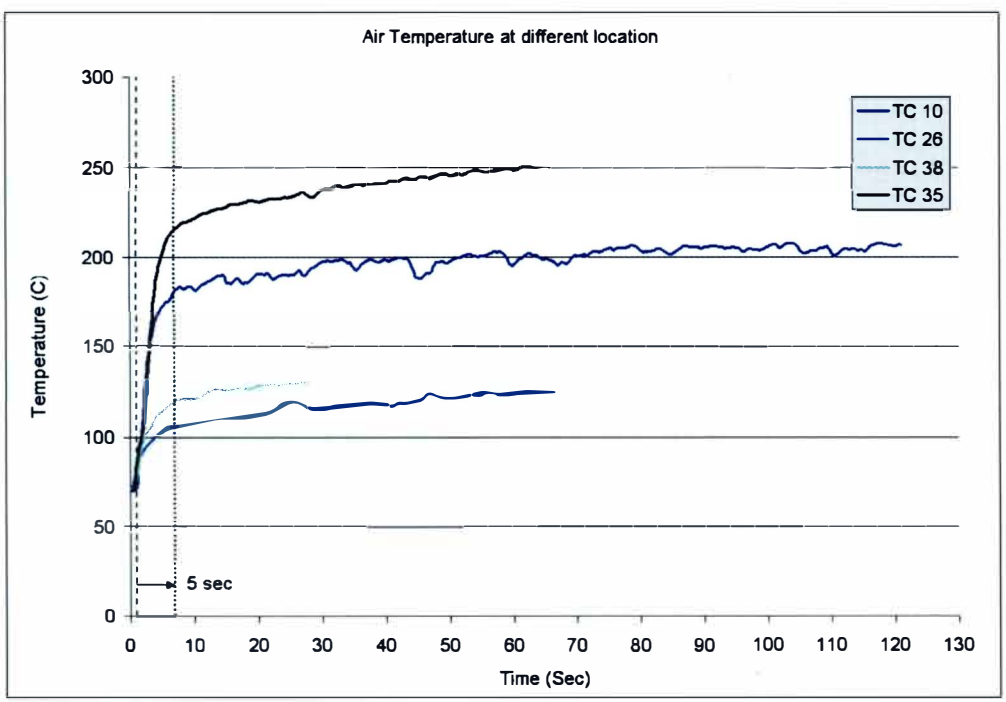

Figure 23. Thermocouple responses at several locations.

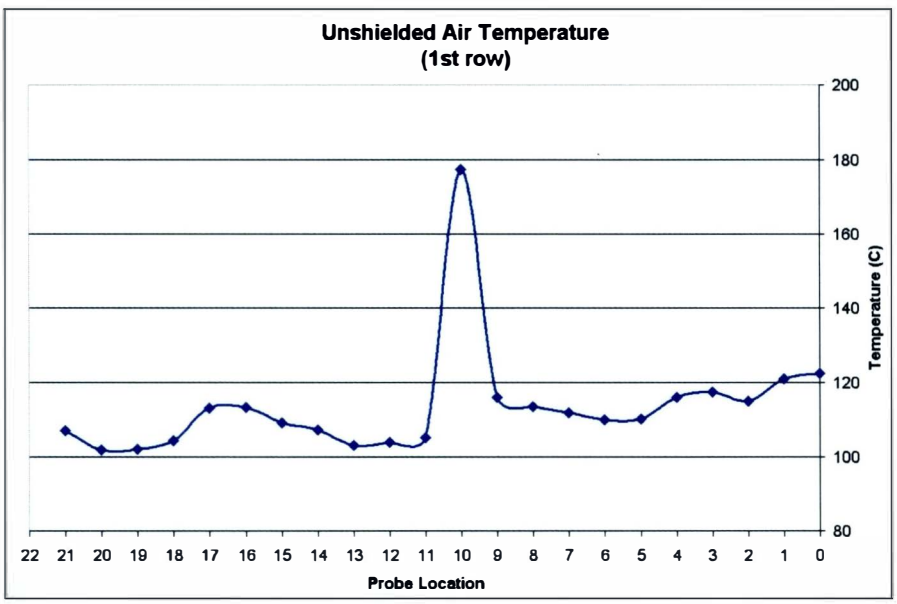

Figure 24. Top row air temperature profile.

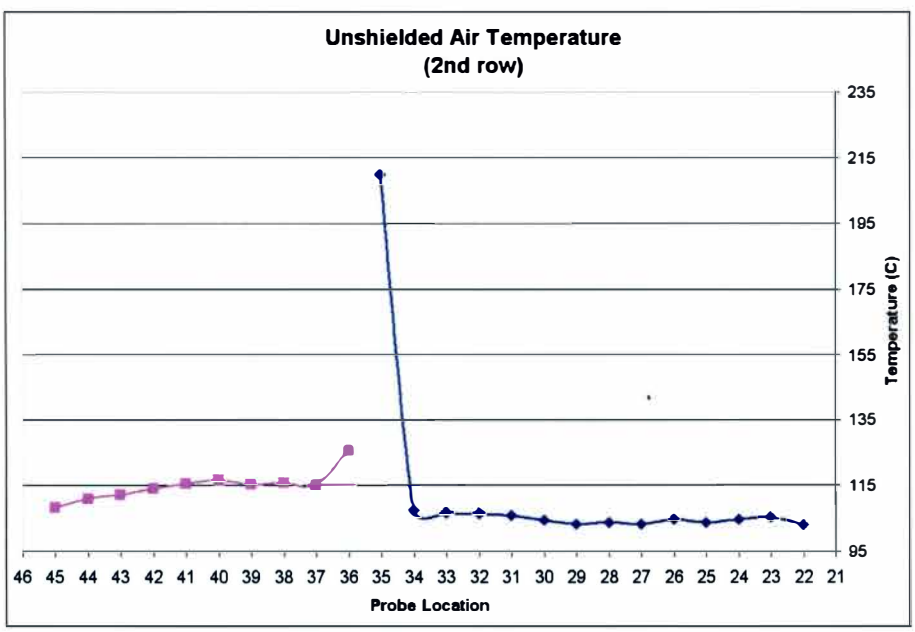

Figure 25. Second row air temperature profile.

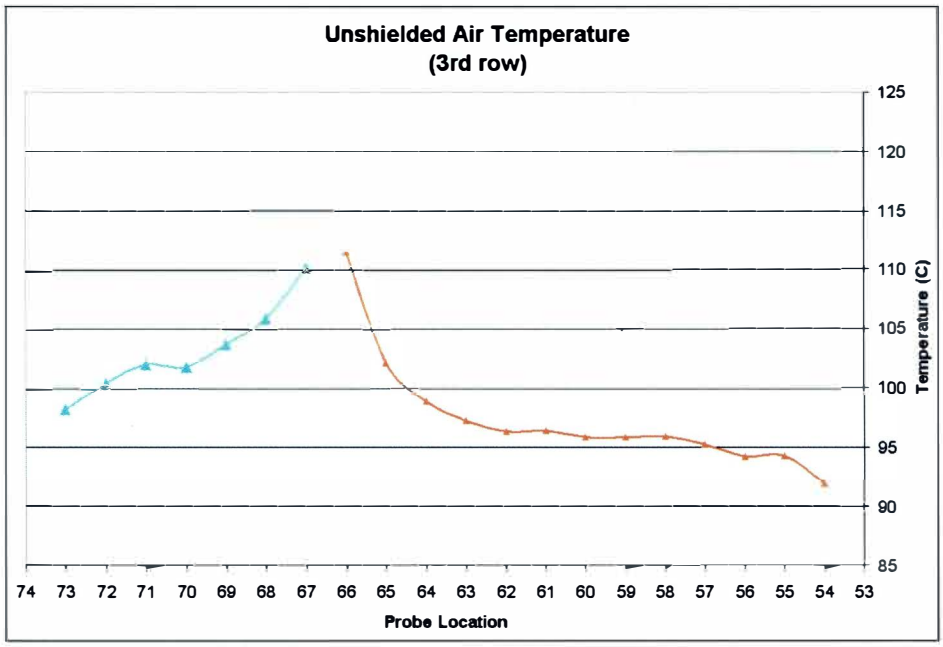

Figure 26. Third row air temperature profile.

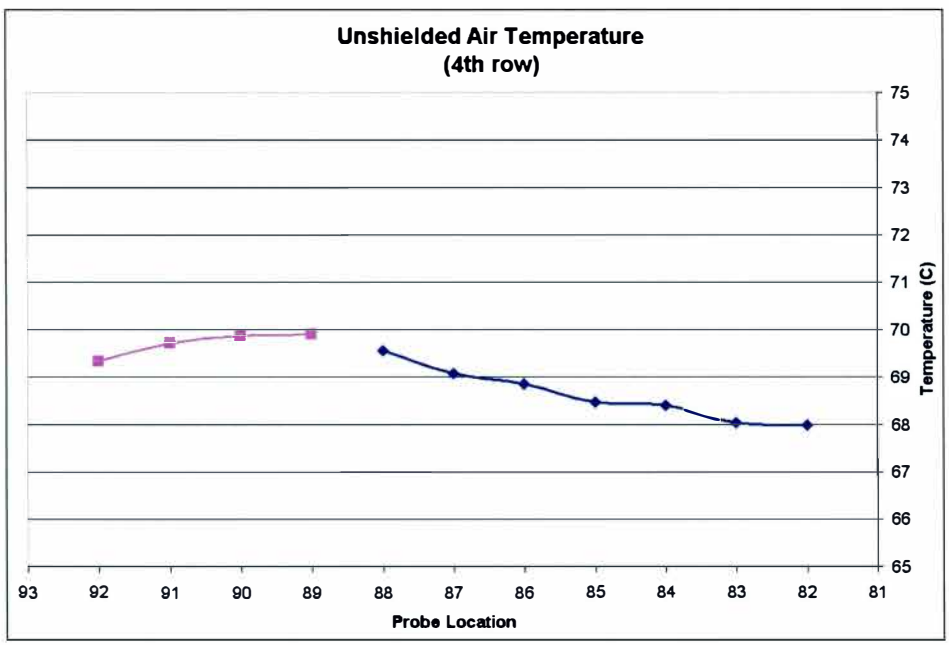

Figure 27. Fourth row air temperature profile.

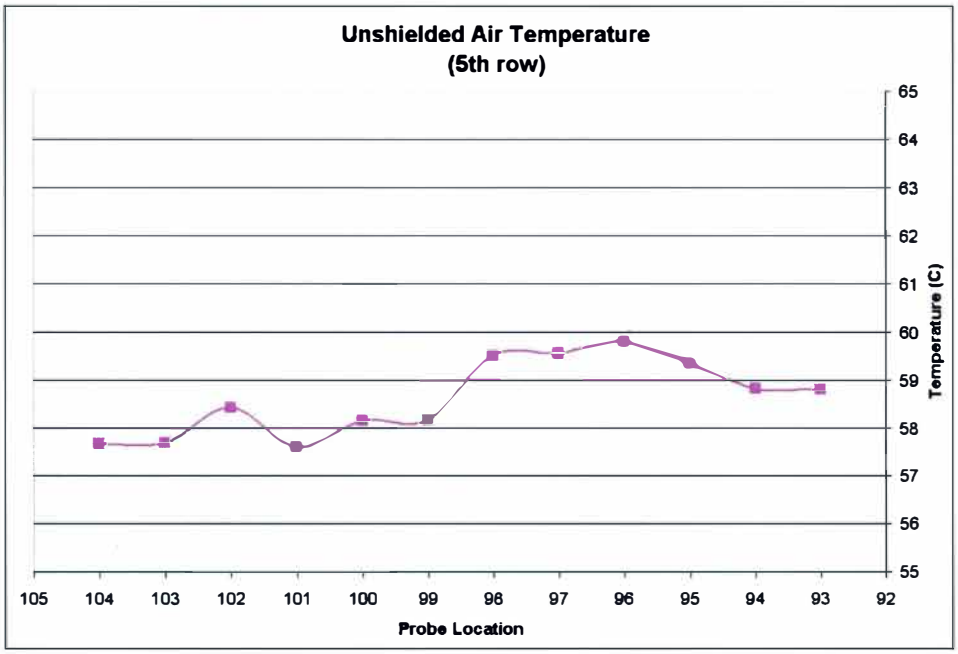

Figure 28. Bottom row air temperature profile.

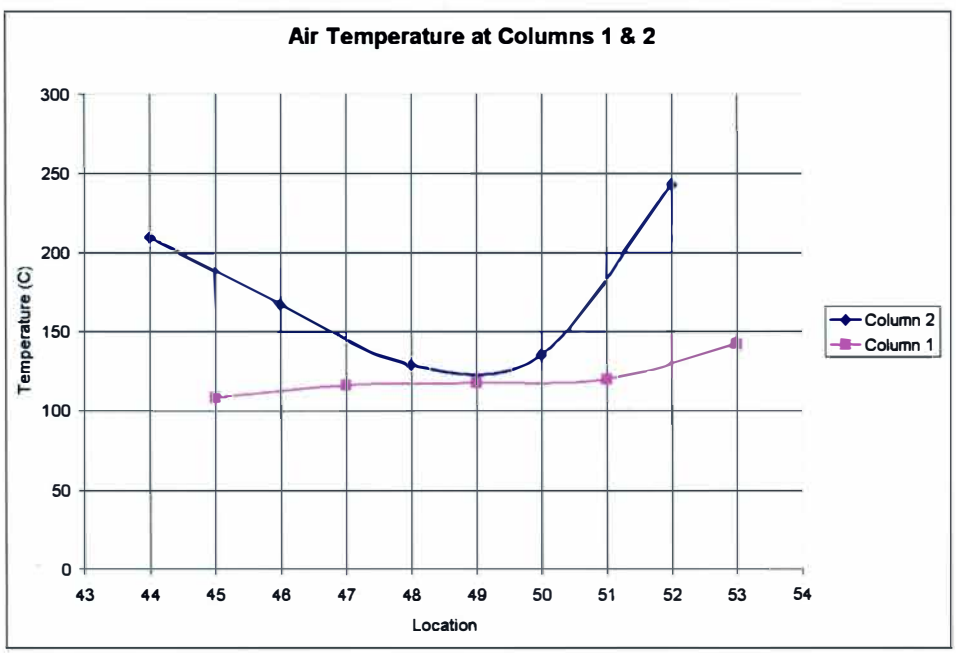

Figure 29. Columns 1 and 2 air temperature profile.

Particle Image Velocimetry Results

X-Y Planes Velocity Contours

Velocity magnitude and standard deviation contours are displayed in Figure 30 to 34 X-Y planes at all locations. Highest velocity magnitude is located on the top region above the exhaust heaters. Main buoyancy driven flow are located above the exhaust heaters where temperature differences between the surface and surrounding air is the highest generating maximum buoyant force. Hot plume generated creates stagnant regions on the top surface separating the flow into two different directions. Velocity stream traces in the next section will show details of the flow path. The maximum velocity magnitude of 0.75m/s is obtained in X-Y plane of Z=444mm where the temperature of the exhaust heaters were at maximum 600 ^{o}C. Velocity standard deviations are highest in similar regions. This indicates unsteadiness at high velocity magnitudes regions. Approaching plane at Z=686mm, fluctuation of the flow in these top regions became increasingly wide spread. At Z=736mm velocity magnitude reduced to 0.35m/s as the unsteadiness filled the top region above the heaters. The out of plane motion becomes significant moving away from the center of the engine block which is shown in Figures 35 to 38 for Y-Z planes locations.

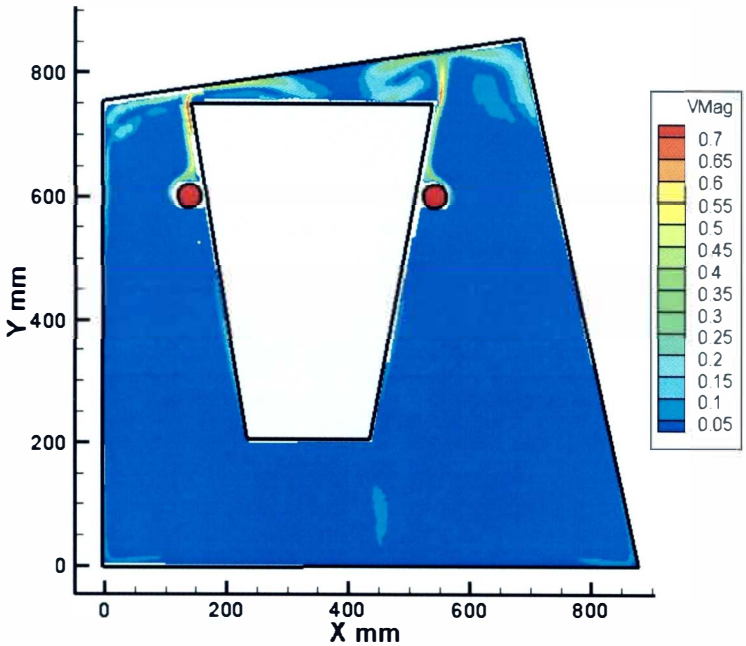

(a). Velocity magnitude contours.

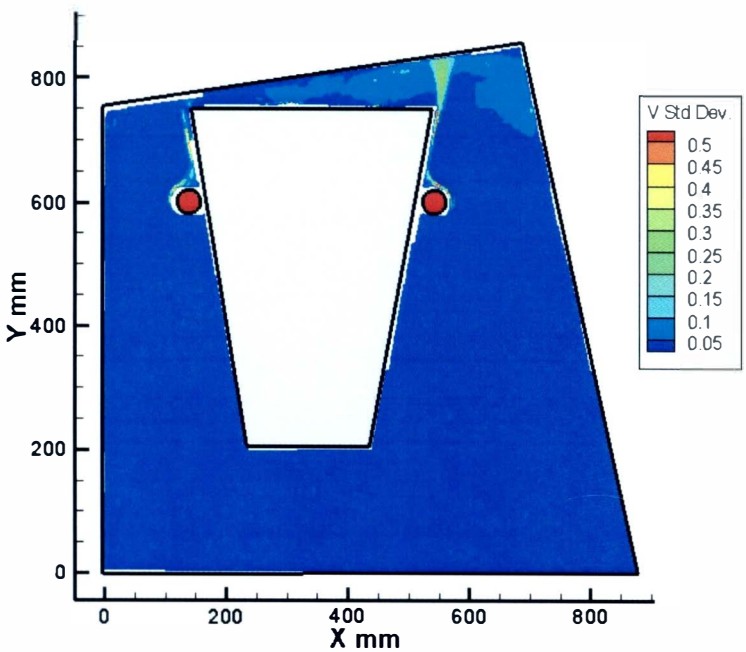

(a). Velocity standard deviation contours.

Figure 30. X-Y plane at Z = 317mm with (a) Velocity magnitude contours, (b) standard deviation contours.

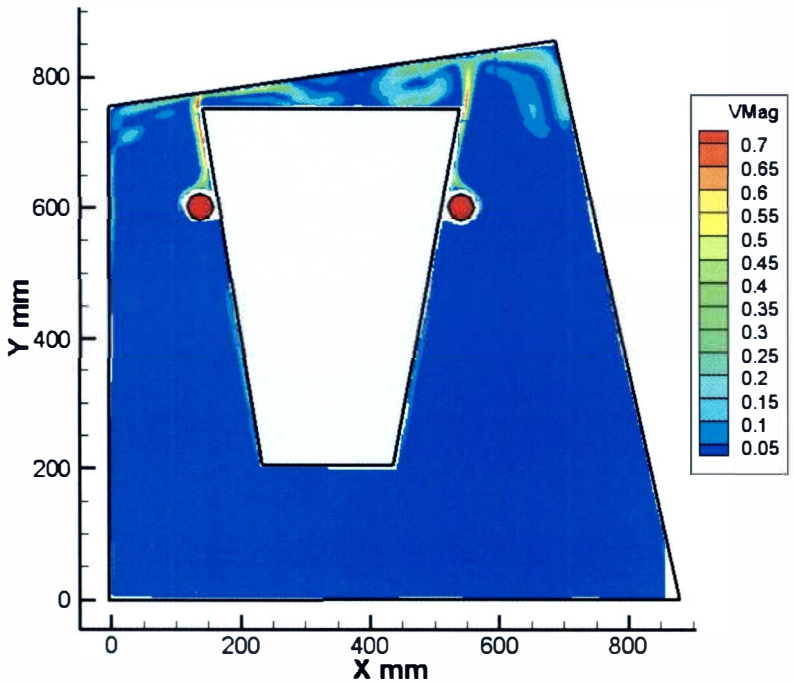

(a). Velocity magnitude contours.

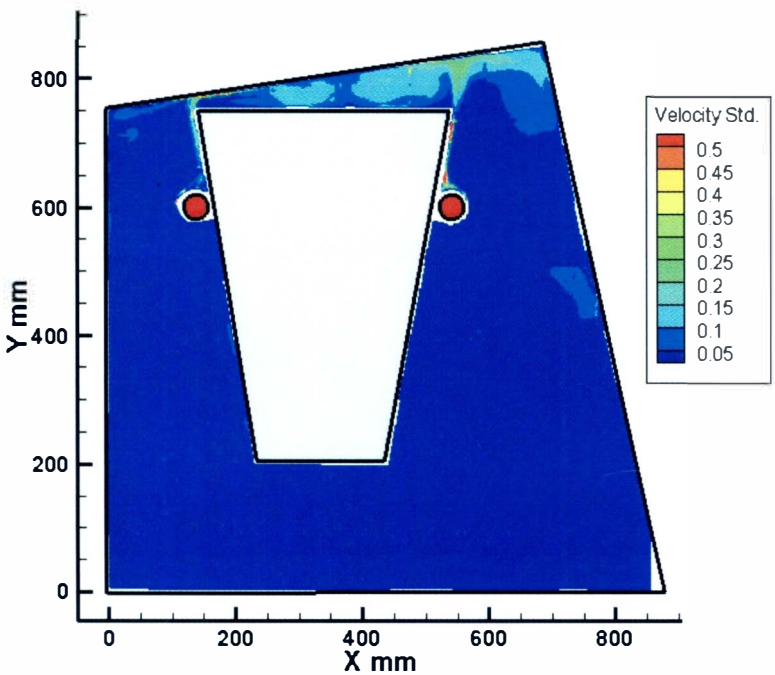

(a). Velocity standard deviation contours.

Figure 31. X-Y plane at Z = 444mm with (a) Velocity magnitude contours, (b) Velocity standard deviation contours.

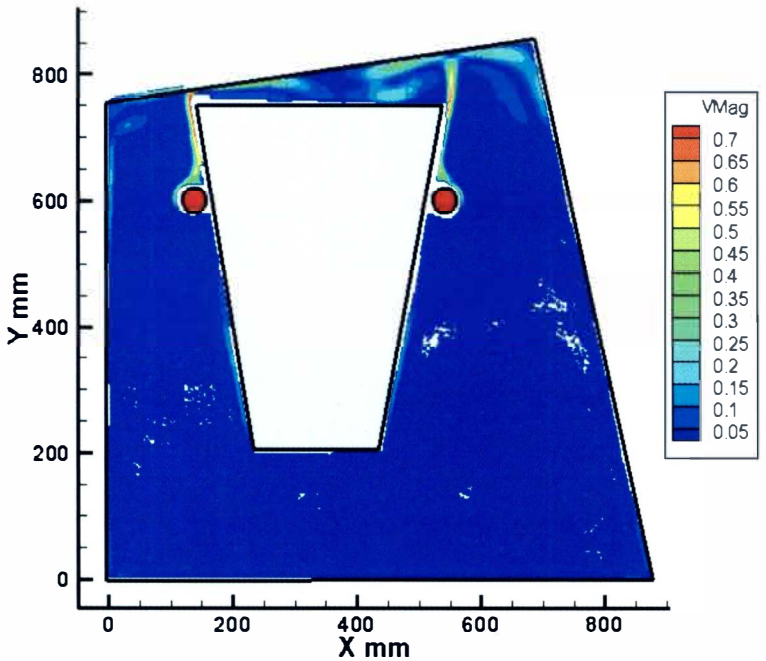

(a). Velocity magnitude contours.

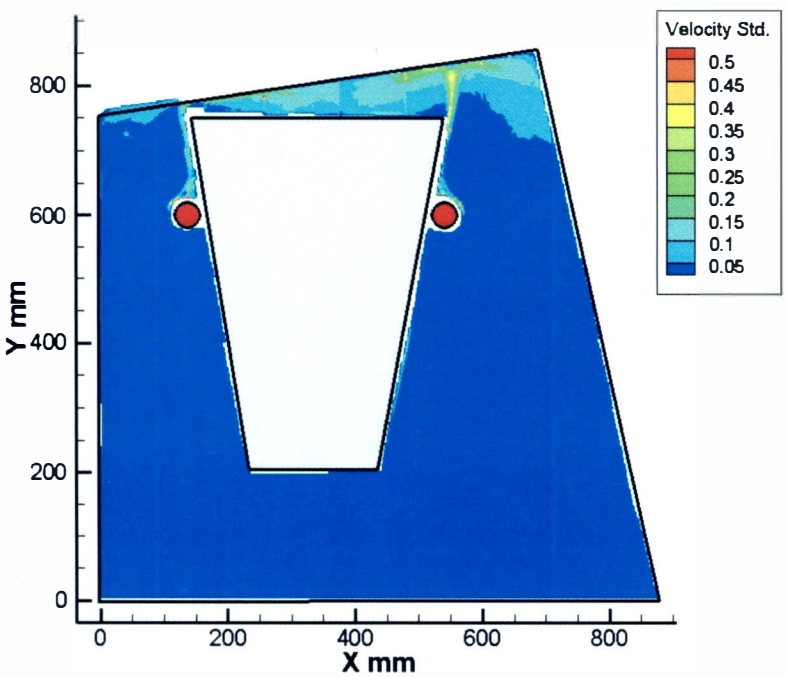

(a). Velocity standard deviation contours.

Figure 32. X-Y plane at Z = 571mm with (a) Velocity magnitude contours, (b) Velocity standard deviation contours.

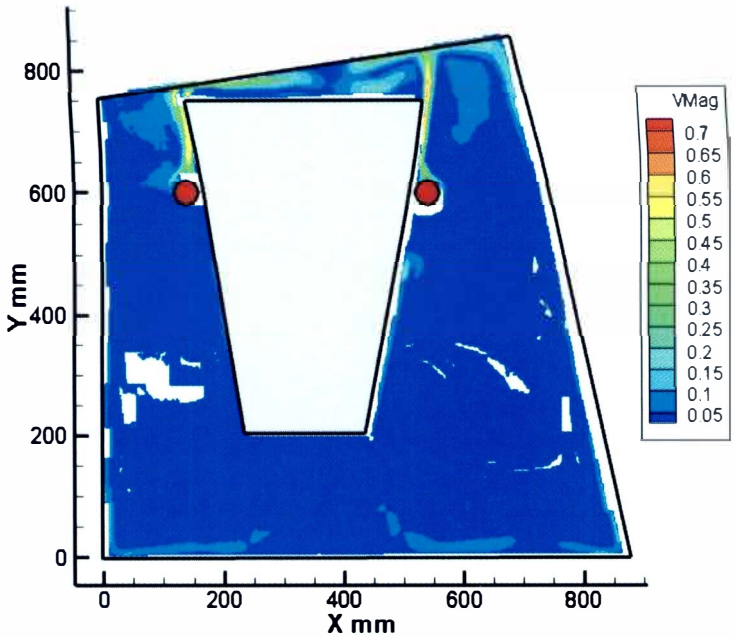

(a). Velocity magnitude contours.

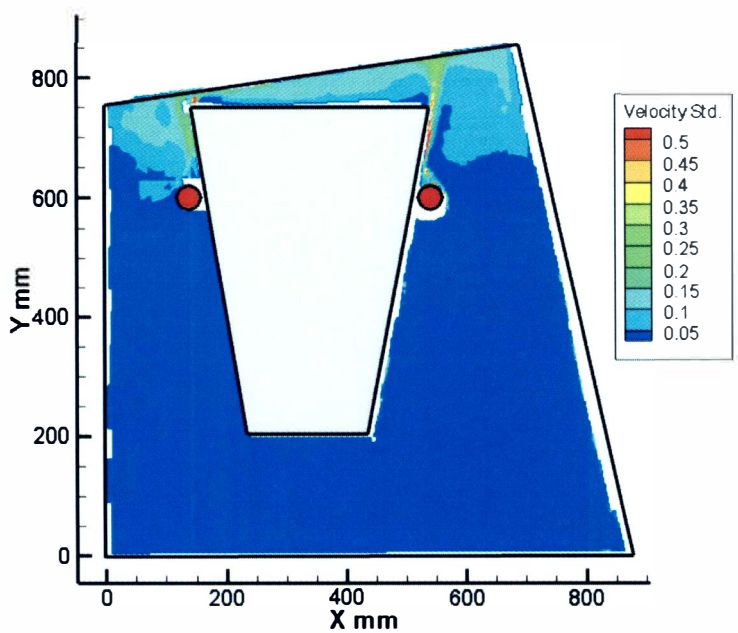

(a). Velocity standard deviation contours.

Figure 33. X-Y plane at Z = 686mm with (a) Velocity magnitude contours, (b) Velocity standard deviation contours.

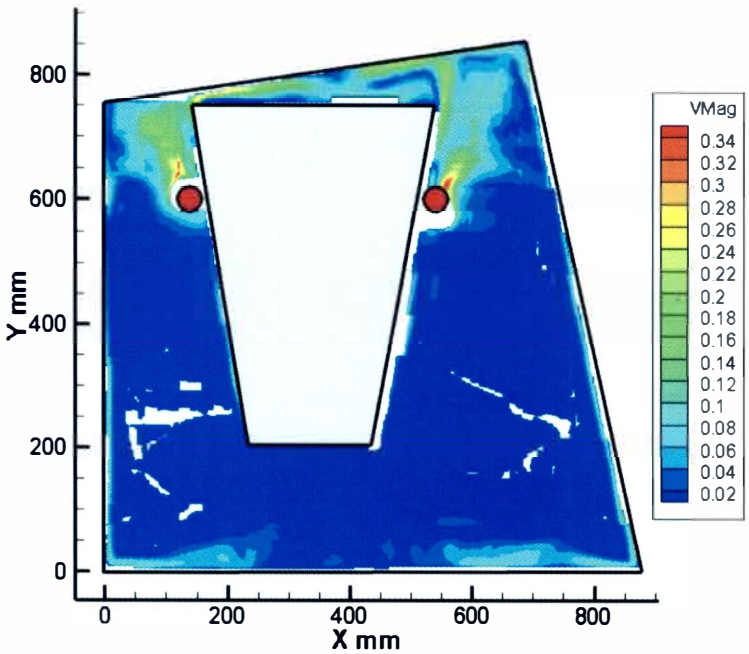

(a). Velocity magnitude contours.

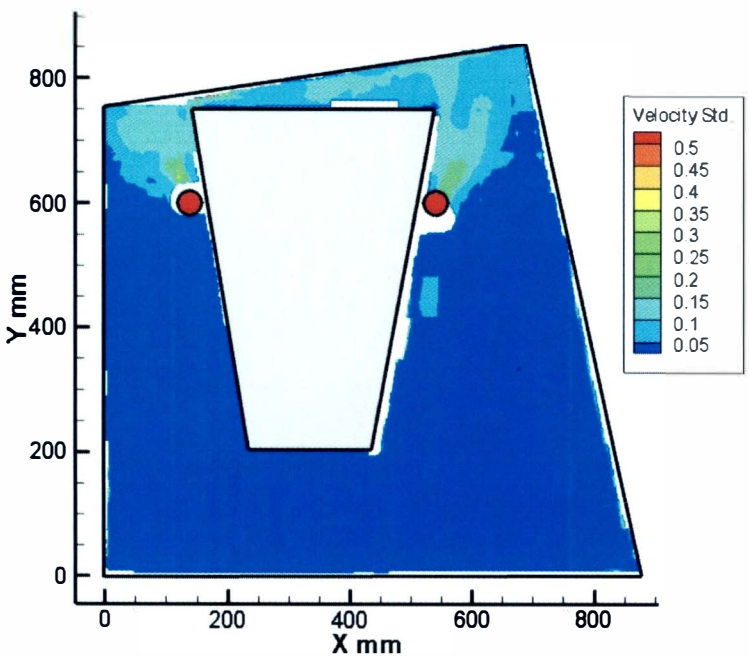

(a). Velocity standard deviation contours.

Figure 34. X-Y plane at Z = 736mm with (a) Velocity magnitude contours, (b) Velocity standard deviation contours.

Y-Z Planes Velocity Contours

Figures 35 to 38 show velocity magnitudes and standard deviation contours of the Slant plane and Y-Z planes at different locations. An outline sketch of the engine block and exhaust heater within the plots is added. At plane X=15mm shown in Figure 36, large velocity magnitudes are present on all sides in proximity of the glass casing. Stream tracers in later section will show that these high velocities are a result of flow recirculation and cooling. Velocity fluctuations are found only on the top and both sides of the enclosure. Velocity deviation increases as the flow move away from the center of the engine block. This is consistent to X-Y planes at locations closer to the front of the engine block where fluctuations built up enveloped the top regions of these planes.

Figure 37 show velocity information of three partial Y-Z planes at three different location. Plane X=236mm has low velocity on the top where majority of the flow is out of plane. Planes X=439mm and X=515mm contain high velocities on the top region since it captures part of the strong vortices generated by the thermal plume from the exhaust heater on the top surface of the engine. In front the engine (left region), a low velocity region exist as result of vortex expansion which will be further discussed. Velocity standard deviation on all three planes are consistent with earlier finds where the flow becomes increasingly unsteady as it travels away from center X-Y plane of Z=337mm in Figure 35.

High velocity magnitudes and deviations are located on the top region of the Slant plane above the heater in Figure 38. Flow recirculation has sustained large magnitudes and deviation of the flow on the top region before being cooled into a down draft on the front and back walls. Higher velocity area on the bottom region of the engine detected suggests dominant flow on the Z direction at this location.

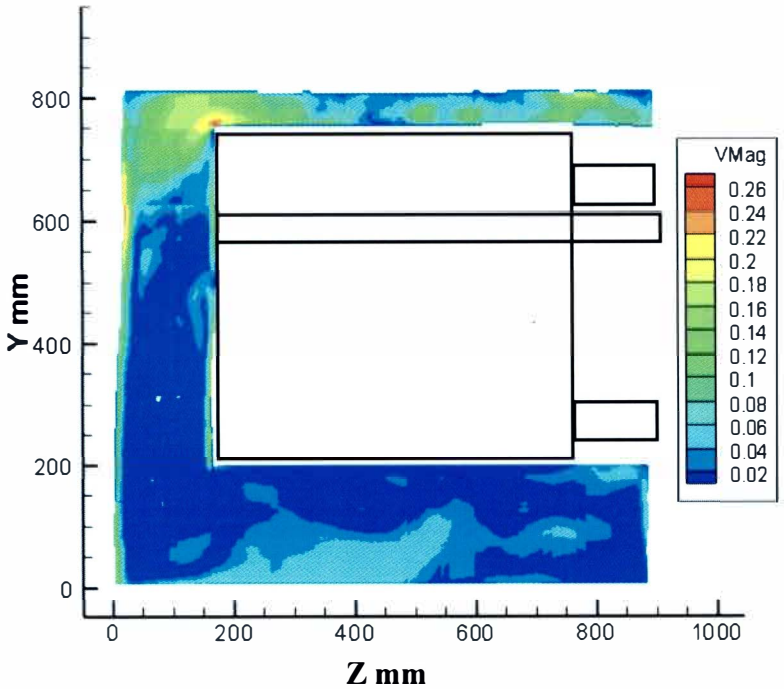

(a). Velocity magnitude contours.

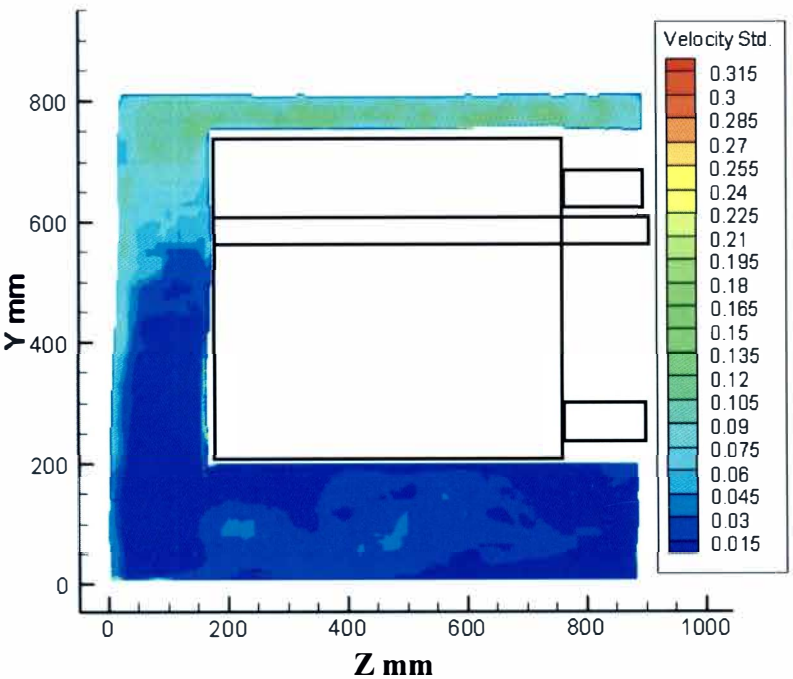

(a). Velocity standard deviation contours.

Figure 35. Y-Z plane at X = 337mm with (a) Velocity magnitude contours, (b) Velocity standard deviation contours.

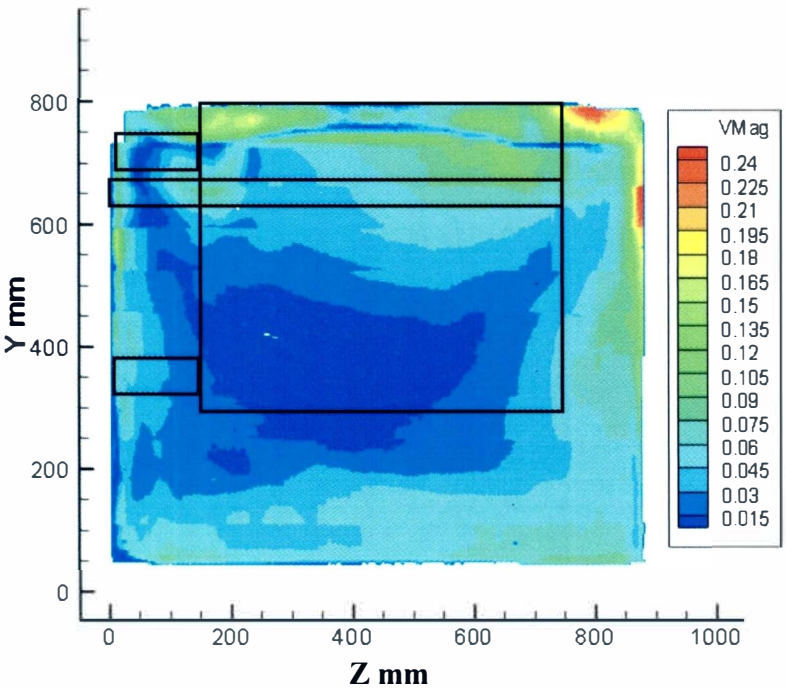

(a). Velocity magnitude contours.

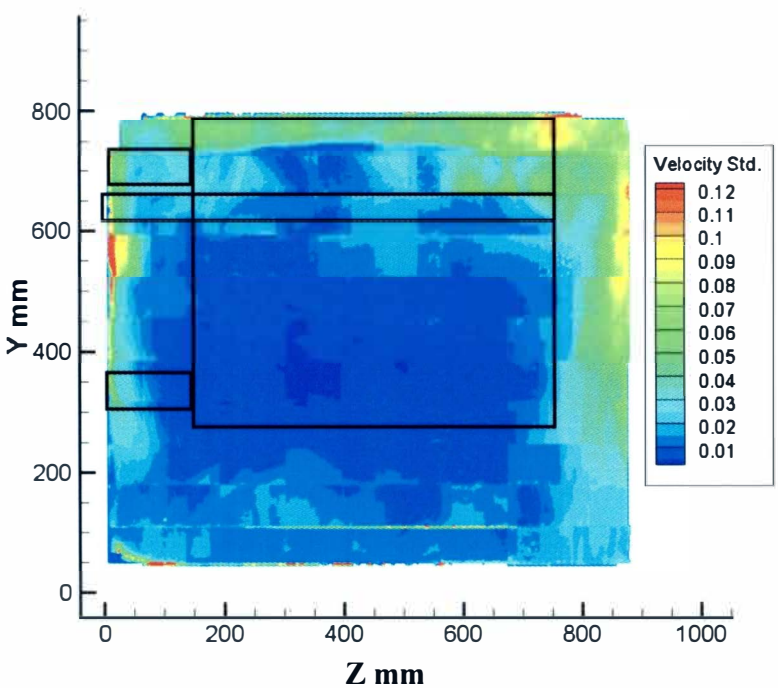

(a). Velocity standard deviation contours.

Figure 36. Y-Z plane at X = 15mm with (a) Velocity magnitude contours, (b) Velocity standard deviation contours.

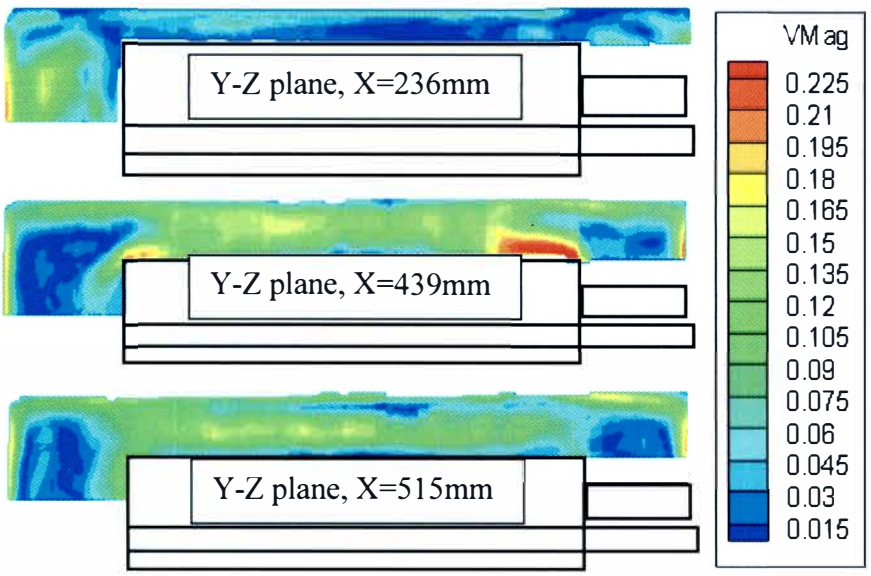

(a). Velocity magnitude contours.

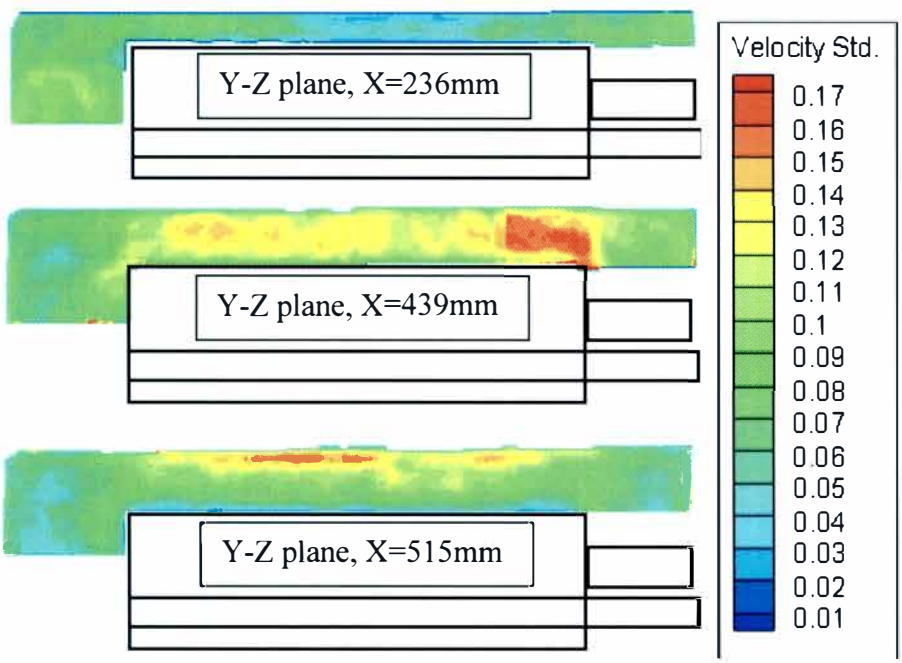

(a). Velocity standard deviation contours.

Figure 37. Y-Z plane at X=236mm, 439mm, and 515mm with (a) Velocity magnitude contours, (b) Velocity standard deviation contours.

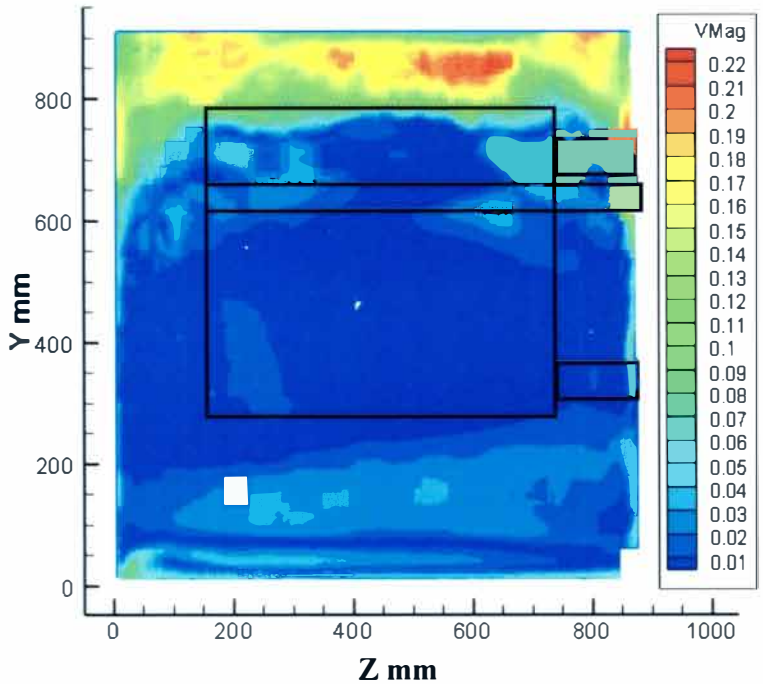

(a). Velocity magnitude contours.

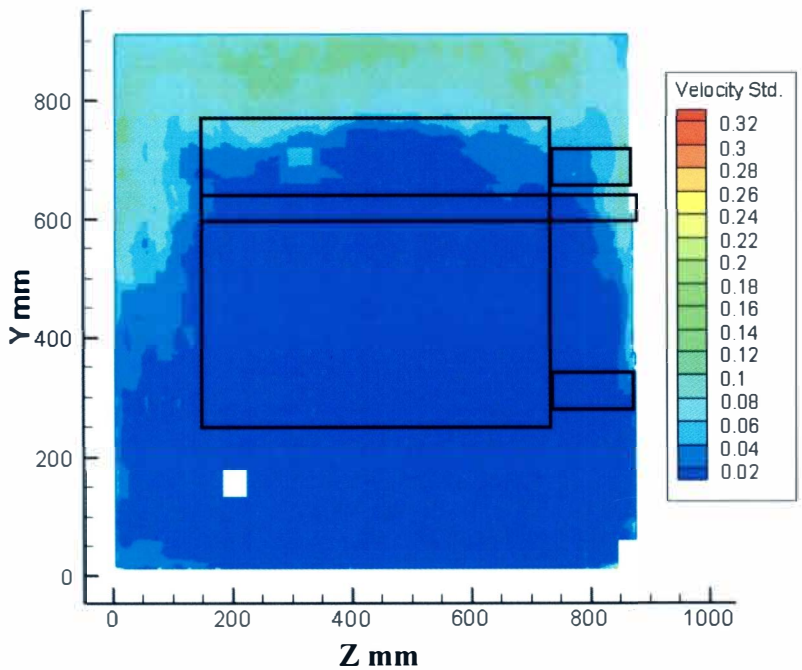

(a). Velocity standard deviation contours.

Figure 38. Slant plane with (a) Velocity magnitude contours, (b) Velocity standard deviation contours.

Velocity Stream Traces

Since the measurements acquired are complex and large in size, different regions will be discussed at a time. The measured X-Y planes will be divided into four regions as shown in Figure 39 which consist of top, left, right, and bottom region. Flow structures driven by the buoyancy force from the exhaust heaters will be clearly revealed. Y-Z planes discussed in later sections will reveal the three dimensionality of flow. Stream tracer function from Tecplot 10 is used to display velocity results.

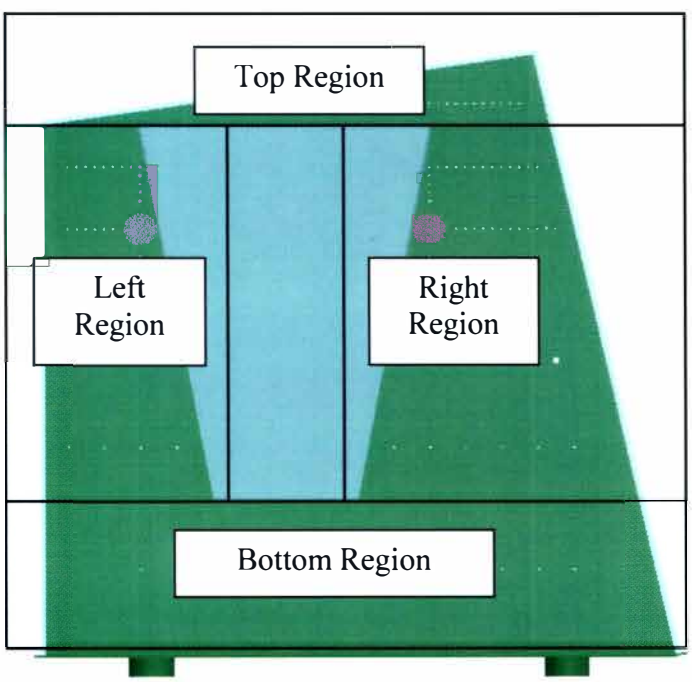

Figure 39. X-Y plane regions.

X-Y Planes Velocity Stream Tracers

Top Region

X-Y planes will be discussed in the increment values of Z that were measured from the support wall. At Z = 317mm in Figure 40, four vortices, two on each side were generated from the hot plume separation upon impingement to the top surface. Plumes on both sides generated clockwise and counter-clockwise rotation vortices. Vortex 1 and 2 are smaller in size compare to vortex 4 and 5 due to the asymmetry of the setup. Larger area between the engine and the top surface allowed larger recirculation. Vortex 5 is formed by the combination of strong flow separation of the thermal plume that forced a downward motion on right surface and an updraft buoyant air resulted from the radiation heated glass surface forced recirculation on the downward motion flow. Vortex 1 and 4 is formed by similar motion where vortex 1 rotates in the opposite direction. Large magnitude of velocity from the left exhaust heater is diverted by the slope of the top glass enclosure to the top of the engine. The highly buoyant flow travels along the top glass surface at large velocity magnitudes created separation on the left engine block top surface where vortex 2 formed.

Z = 444mm in Figure 41 is located at the middle of the engine block. Flow structures are very similar to Z = 317mm where vortex 1, 2, 4, and 5 are sustained. A smaller vortex 3 formed between vortex 2 and 4. The formation of this vortex is unclear but suspected to be driven by surface temperature difference between the surfaces and pressure built up from both sides of the vortices created an almost stagnant region. In Z = 571mm, size of vortex 3 was reduced due to the out of plane motion of the flow which will be discussed in later section.

Approaching the front at Z = 686mm (Figure 41) and Z = 736mm (Figure 42),

drastic changes in the flow were apparent. Size of vertex 1 is reduced and later destroyed by the upward draft. Vortex 5 is separated into two smaller vortices which later almost none existence. Closing to the front edge of the engine block, flows are no longer 2 dimensional. Combining measurements on these X-Y planes with Y-Z planes in later sections the three dimensionality of the flow are defined.

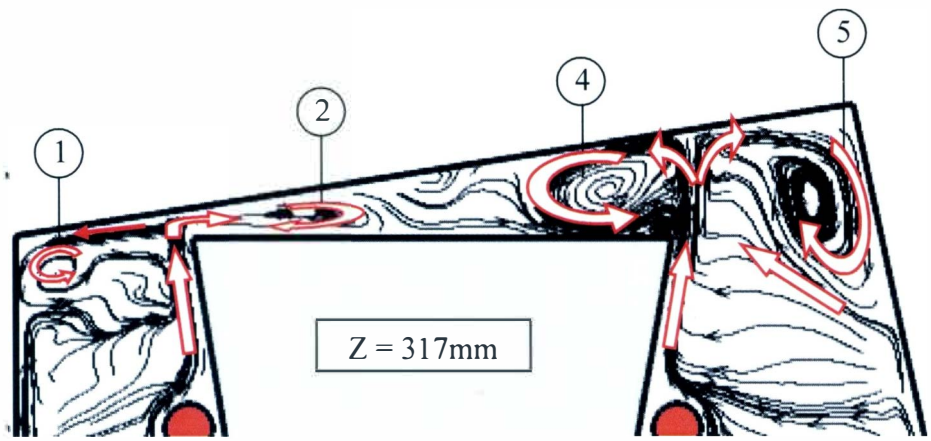

Figure 40. Velocity stream tracers of top region in X-Y plane at Z = 317mm.

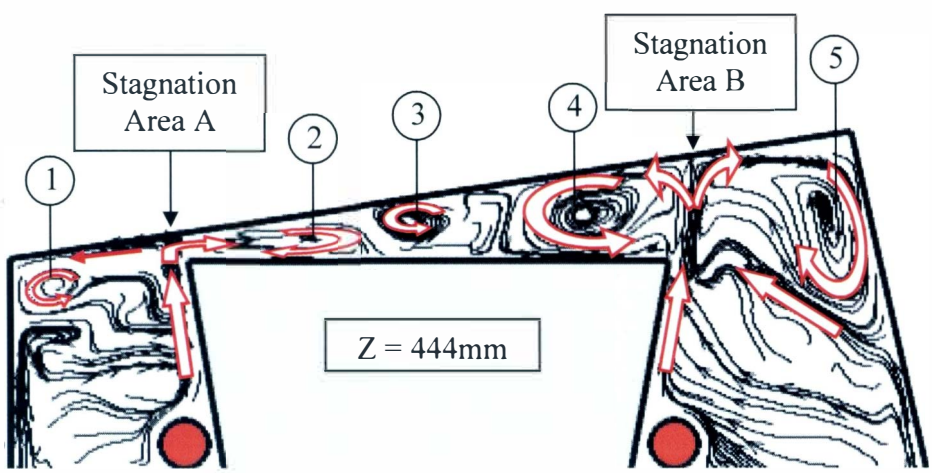

Figure 41. Velocity stream tracers of top region in X-Y plane at Z = 444mm (middle location of the engine block).

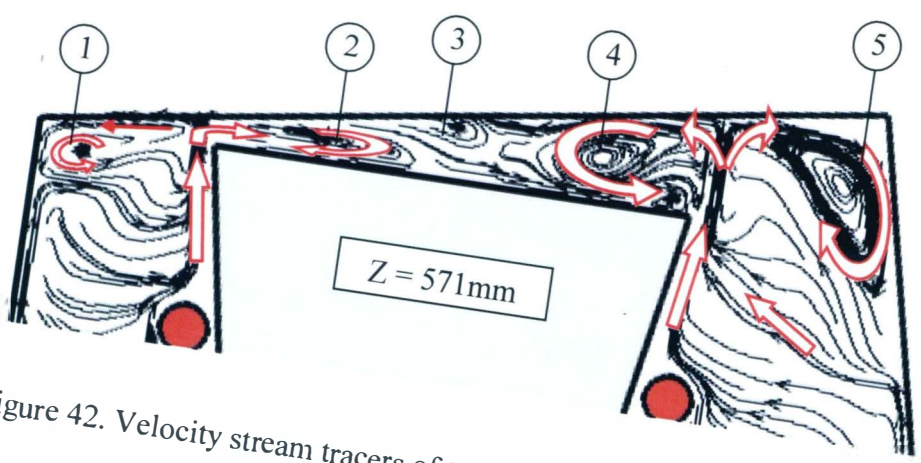

Figure 42. Velocity stream tracers of top region in X-Y plane at $Z = 571$mm.

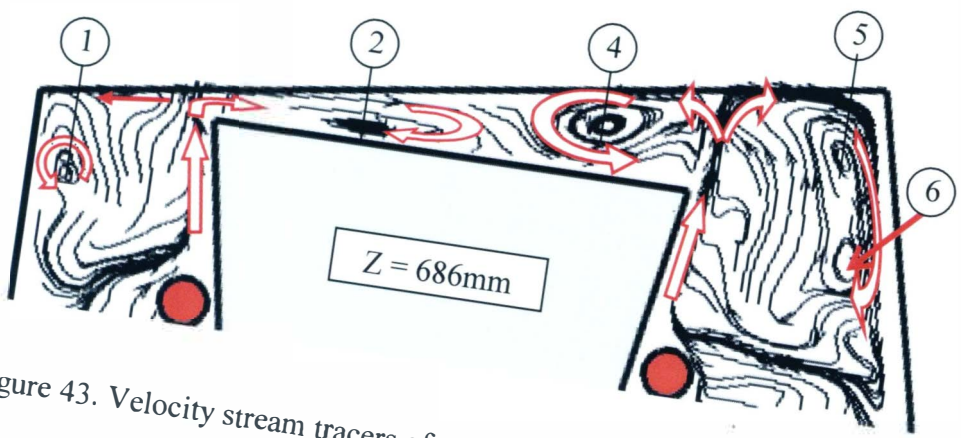

Figure 43. Velocity stream tracers of top region in X-Y plane at $Z = 686$mm.

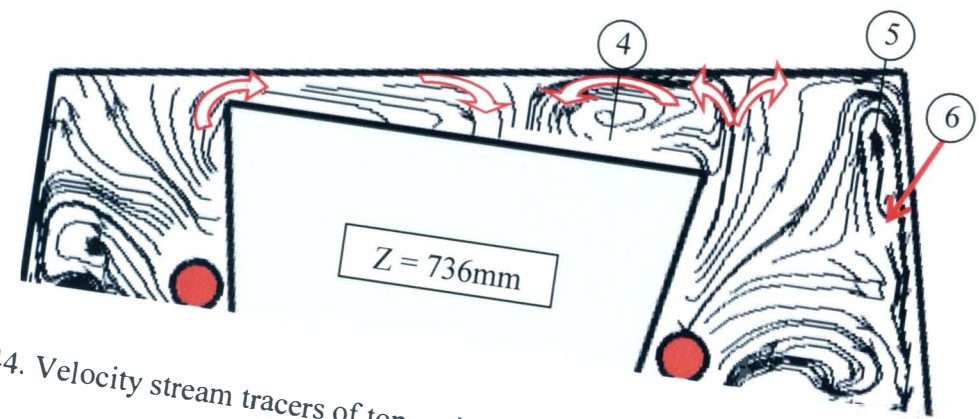

Figure 44. Velocity stream tracers of top region in X-Y plane at $Z = 736$mm (front surface of engine block).

Left Region

Since the top portion in these regions has been discussed early, the main focus in on a stagnation region labeled D and air flows from the engine surface. All five X-Y planes are displayed in Figure 45 where stagnation point C and D are indicated. Stagnation point C is resulted from collision of buoyant air from the hot glass surface and the recirculation from vortex 1. Stagnation point D, however, are resultant of jet like flow impingement onto the glass surface. Moving pass plane Z = 571mm, stagnation points C and D shifts towards each other are resulted from non-uniform and lower glass surface temperatures nearing the front of the engine.

The inclined engine block surface with temperatures in the range of 98 ^{o}C generated an updraft of buoyant air from the lower region where air temperatures are in the 60s ^{o}C and 70s ^{o}C. As the updraft approaches the exhaust heater, it detaches from the block surface due to the blockage of the exhaust heater. Large portion of the detached updraft are entrained onto the glass surface between stagnation point C and D where a stronger updraft are created from surface temperatures beyond 120 ^{o}C. Remainder of the detached flow that separated at stagnation point D was sunk into the bottom region by the colder glass surface temperature below 80 ^{o}C.

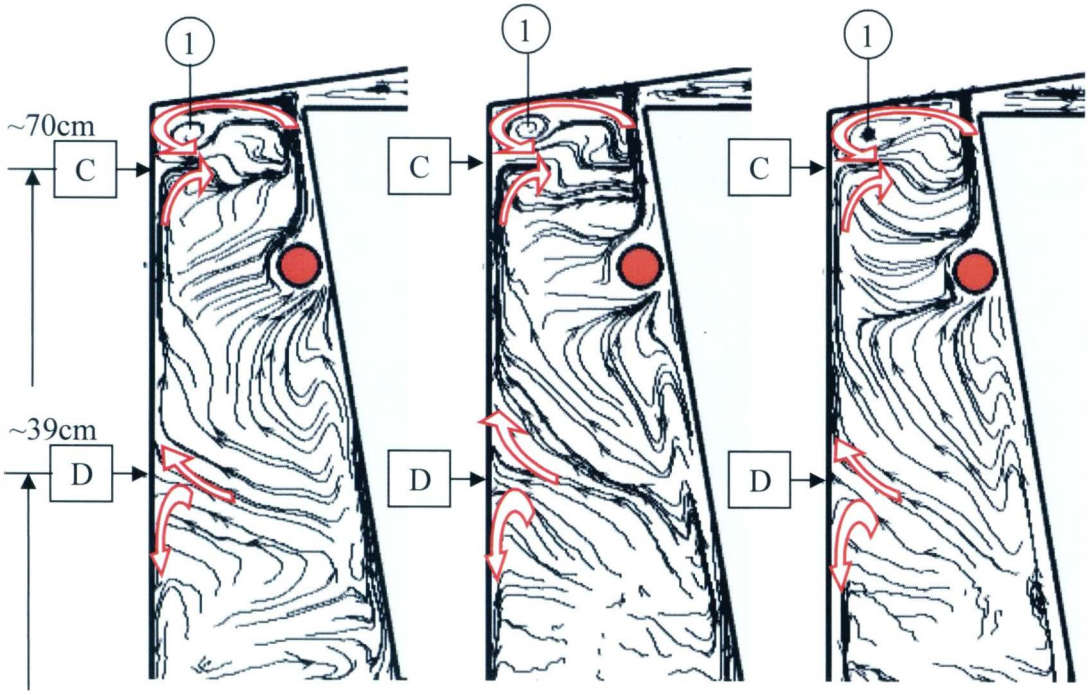

(a) Z = 317mm (a) Z = 444mm (a) Z = 571mm

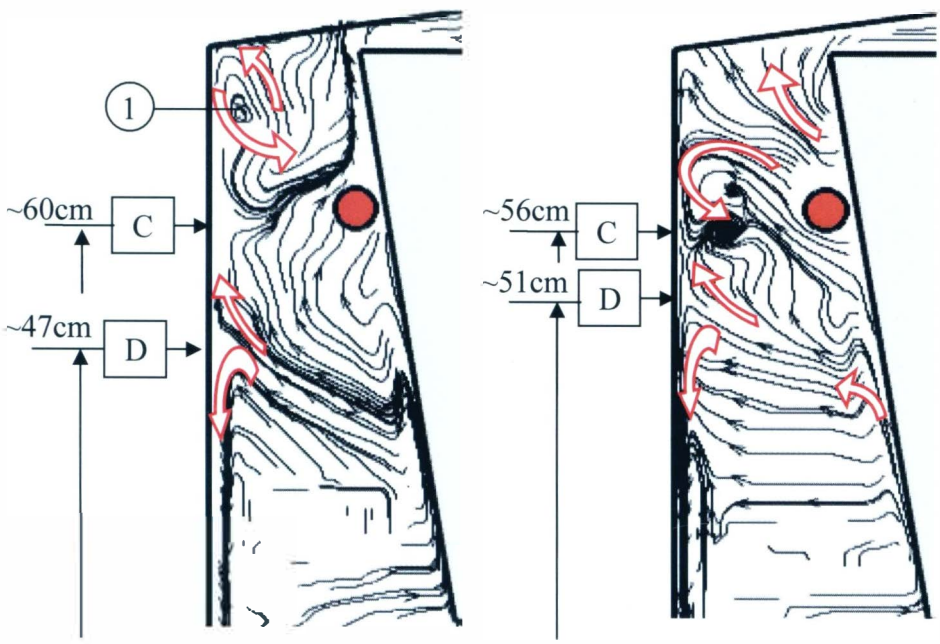

(a) Z = 686mm (a) Z = 736mm

Figure 45. Velocity stream tracers of left regions in all X-Y planes.

Right Region

Flow structures in the right region are very similar to those on the left region. Two different stagnation points E and F were present with similar formation process and stagnation points C and D but in a larger area. Stagnation points E and F vanish in Z = 686mm and Z = 736mm closest to the front region where temperatures on the glass surface turns into a large heat sink. Separation occurs between the engine block and the glass surface as marked in Figure 46 and 47. These are out of plane motion that will be discussed in later section.

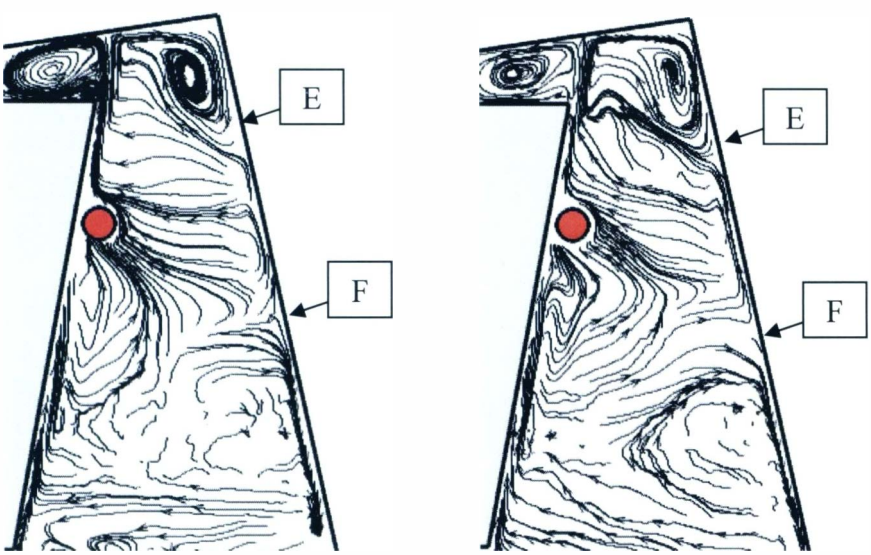

(a) Z = 317mm (b) Z = 444mm

Figure 46. Velocity stream tracers of right regions in X-Y planes (a) Z=317mm, (b) Z=444mm.

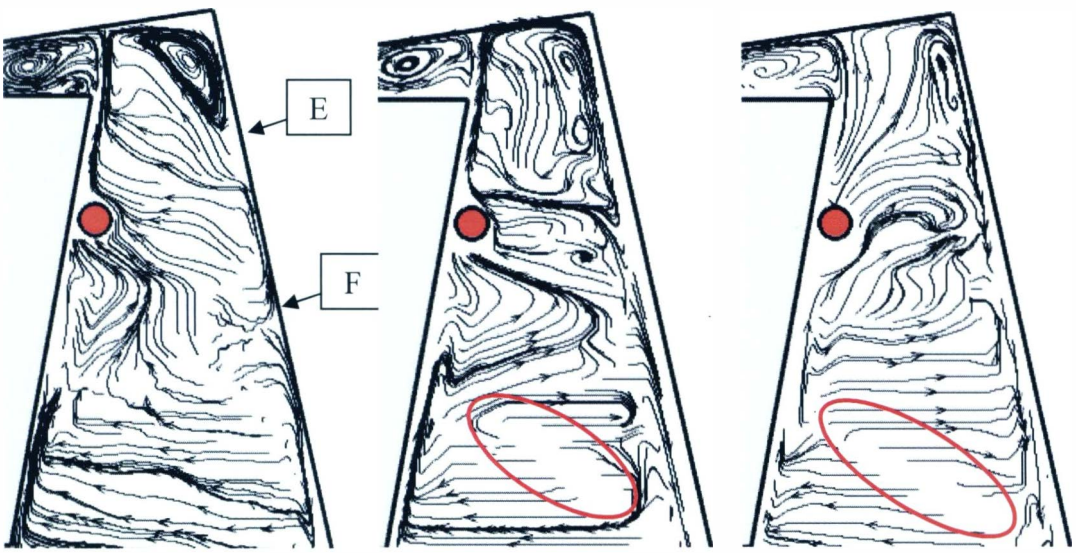

(c) Z = 571mm (d) Z = 686mm (e) Z = 736mm

Figure 47. Velocity stream tracers of right regions in X-Y planes (c) Z=571mm, (d) Z=686mm, (e) Z=736mm.

Bottom Region

Bottom regions of the experimental setup contain velocities of the lowest average magnitudes on the entire measured plane. With the absence of strong convective force in sustaining common flow structures, measurement results vary at different Z locations. Common flow patterns for where found to be located under the lower engine surface and on both corners of the casing. Buoyant flow impingement developed on the bottom surface of the engine block generating another stagnation region. This is due to colder air entrained by the low pressure generated by the accelerating thermal boundary layer that starts from the middle of the engine bottom surface to the side walls of the block. Since this is a weak pressure driven flow from the thermal boundary layer, the stagnation point from the impinging flow varies with the unsteady updraft. On the corners of the enclosure, cooling air sunk by the glass surfaces created a downdraft on both sides. It

continued traveling on the colder aluminum surface until perturbation.

Existence of vortices formed in an almost random manner as indicated in Figure 47(c) and Figure 48(d) will not be discussed due to complexity of its origin and lack of information. Figure 49(e) suggests that more thermal boundary layer has developed on the front surface of the engine block. This is evident in the Y-Z plane.

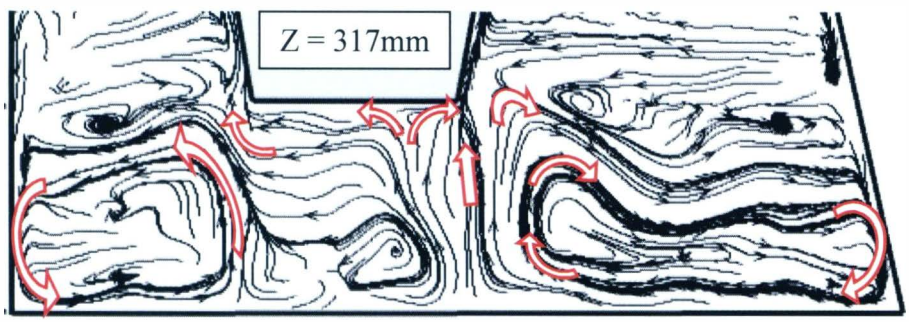

(a) Z = 317mm

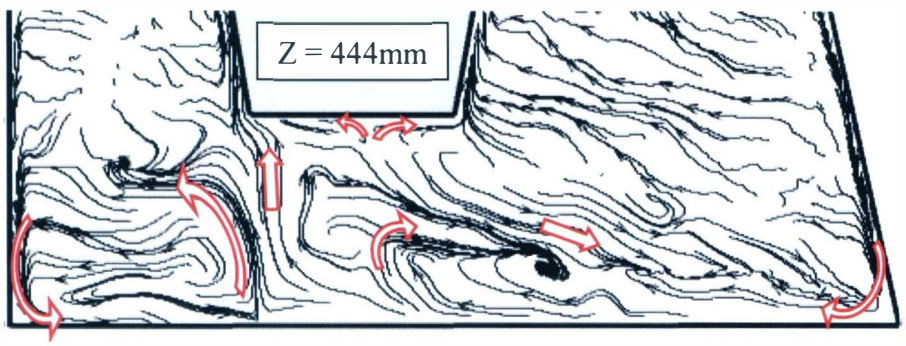

(b) Z = 444mm

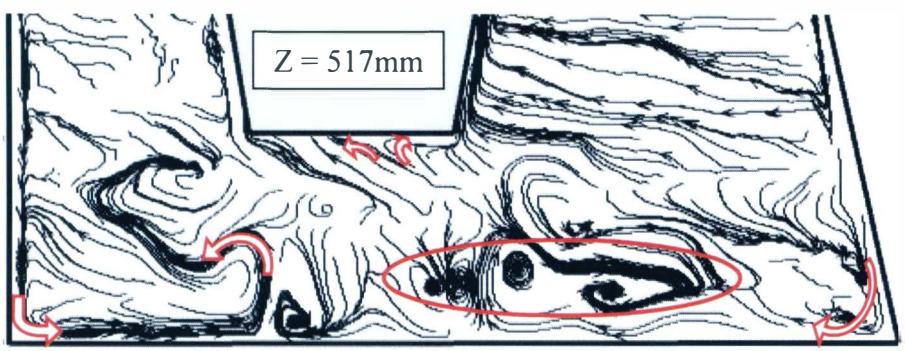

(c) Z = 517mm

Figure 48. Velocity stream tracers of bottom regions in (a) Z = 317mm, (b) 444mm, (c) 517mm of X-Y planes.

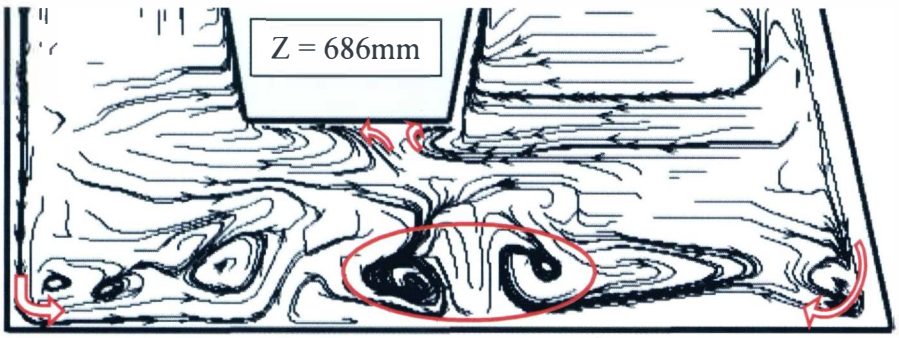

(d) Z = 686mm

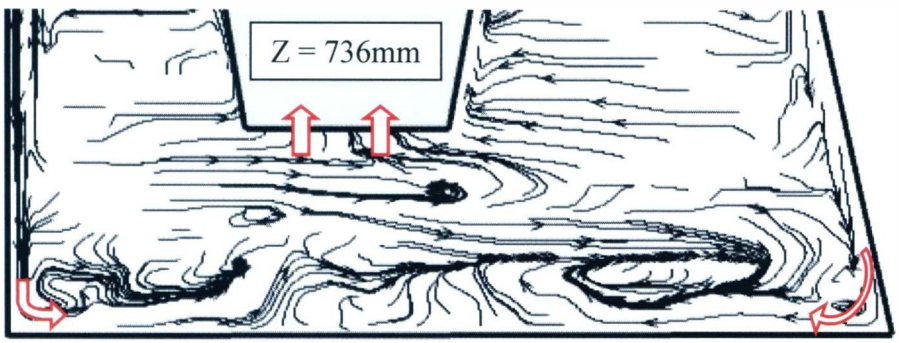

(e) Z = 736mm

Figure 49. Velocity stream tracers of bottom regions in (d) Z = 686mm, (e) 736mm of X-Y planes.

Y-Z Planes Velocity Stream Tracers

Measurements for three partial and two full Y-Z plane acquired at X = 236mm, 337mm, 439mm, and 515mm revealed the third component of the vortices on the top region of the engine block. Figure 50 show locations of these planes slicing thru part of the vortices. Full Y-Z plane will be first discussed and later close comparison of the partial planes.

In plane X=337mm (Figure 51), area labeled A contained common flow pattern that existed in the left and right regions of the X-Y planes where flow recirculation are

created by the source and sink of heat. As the hot air from the top was being cooled on the front glass surface, it travels downwards. Cooled to a certain temperature, partial air separates into vortex 7 and recalculate in area A. This cooler air is then entrained onto the rising thermal boundary layer on the engine front surface. The buoyant updraft then separates in a similar pattern as those below the exhaust heaters on X-Y planes but in absence of the heaters as obstruction. Instead, it collided with the downdraft of hot air forcing the formation of vortex 7 and another stagnation point E.

Above the engine block top surface, the third component of vortex 2 is revealed. Clockwise rotation of vortex 2 travels both forward and backward with increased pitch approaching the ends for the engine block. Figure 52 shows an illustration of an approximated path of vortex 2, 4, and 5. On the front of the engine block, vortex 2 will be expanded into a downward motion and into a larger rotation to sudden area expansion. The rotating motion is sustained by the strong buoyancy force of the exhaust heater where vortex 4 experiences similar phenomena of vortex 2.

Vortex 2 in partial Y-Z plane of X=236mm in Figure 53(a) is suspected to be part of the same vortex 2 in X-Y planes generated from the expansion. Downward motion of the flow in Figure 53(b) and the up drafting flow in Figure 53(c) matched rotation of vortex 4 where it was sliced. When vortex 4 expanded in front of the engine, a low pressure region was exposed where low vortices were formed.

Y-Z plane at X = 15mm in Figure 54 is the closest possible measurement plane to the left glass surface. The details of the stagnation points C and D are clearly shown. The curving of these stagnation regions is cause mainly by the surface temperature of the glass enclosure as shown Figure 55. Uneven heating on the ends of the exhaust cylinder created high temperature regions in the middle of the surface and lower temperatures on the ends of the left glass surface. Radiation emanating from the exhaust heaters is the main source of heating on both sides of the glass surfaces. Therefore, glass surface temperature is

higher then the air temperature around this area which generated such unique air flow pattern.

Counter rotating flow from the left and right upper corners are extended result of vortex expansion on the front of the engine. Similar counter rotating is also present in the slant plane measurement which was recorded at a distance of 24mm parallel to the slant surface shown in Figure 56. A stagnation region is also detected as SL3. The distance of 24mm parallel to the slant surface was too far from thermal boundary layer to capture curving of the stagnation region.

Compiling all the main flow structures analyzed the flow structures in the enclosure can be generalized by sketches in Figure 57. There are three large 3-Dimensional vortices on the top region. These vortices changed into secondary vortices at the four corners of the engine block shown in Figure 57(a). At the front engine block surface, rotation of the vortices forced a downward flow motion creating a stagnation region both on the front glass and engine block front surface. Uneven heating of the left glass surface caused complex flow stagnation area. By successfully interpreted 3D effect of the flow field in the enclosure this research is a success.

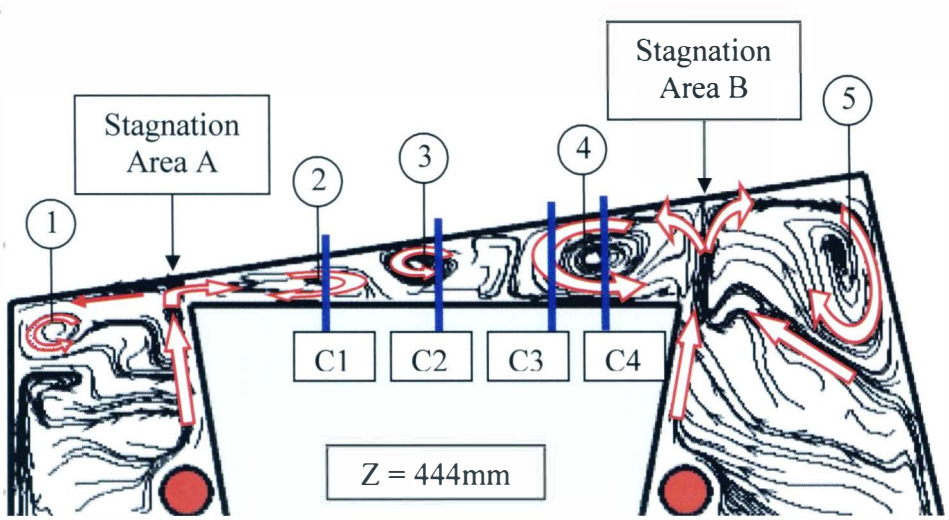

Figure 50. Location of Y-Z planes at X=236mm (C1), 337mm (C2), 439mm (C3), and 515mm (C4).

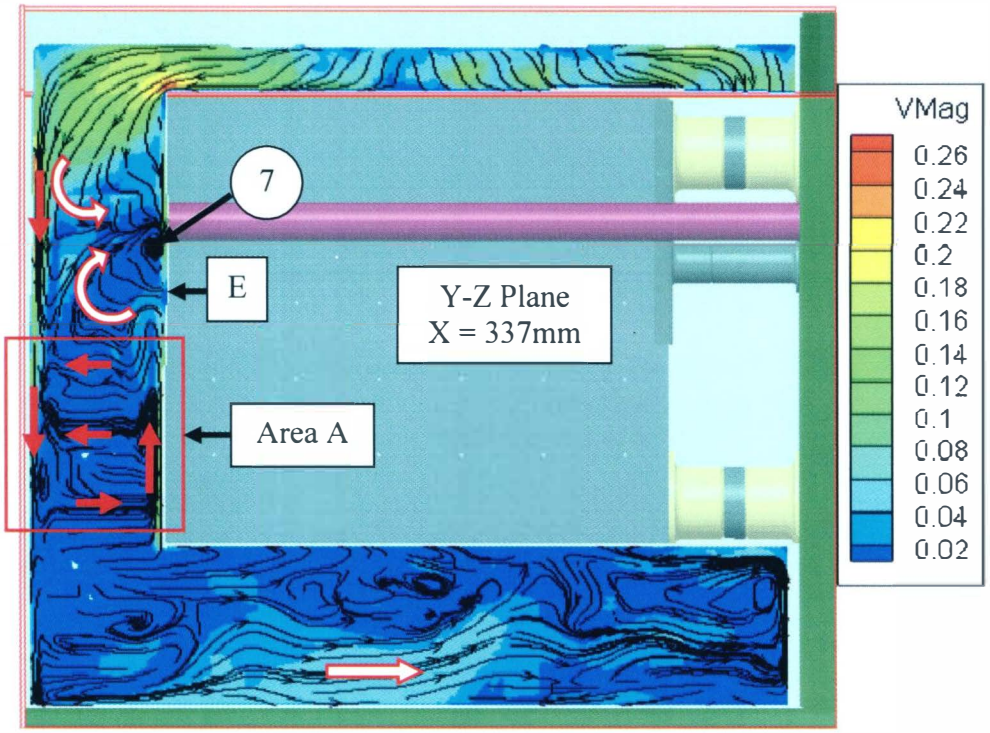

Figure 51. Velocity stream tracers of Y-Z plane at X = 337mm.

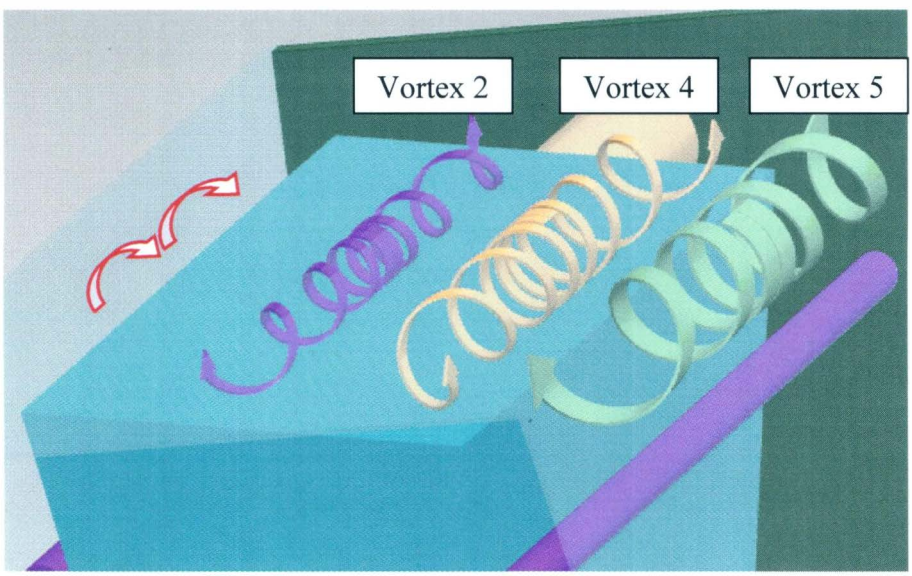

Figure 52. Approximated 3-D vortices.

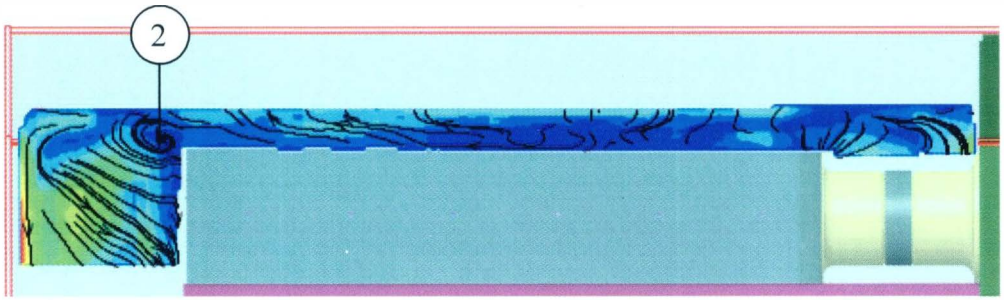

(a). X = 236mm.

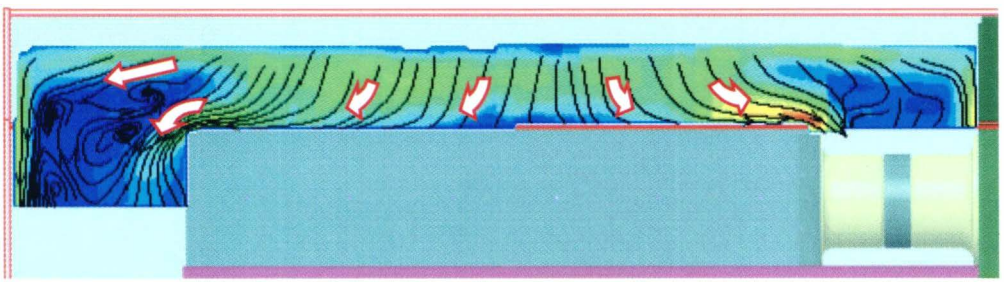

(b). X = 439mm.

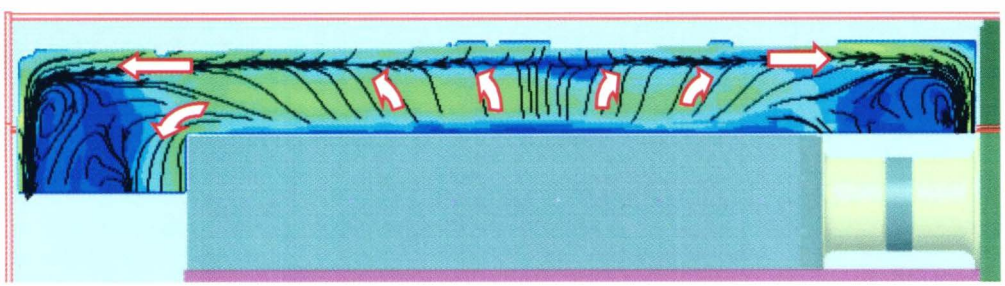

(c). X = 515mm.

Figure 53. Velocity stream tracers of partial Y-Z planes (a) X=236mm, (b) X=439mm, (c) X=515mm.

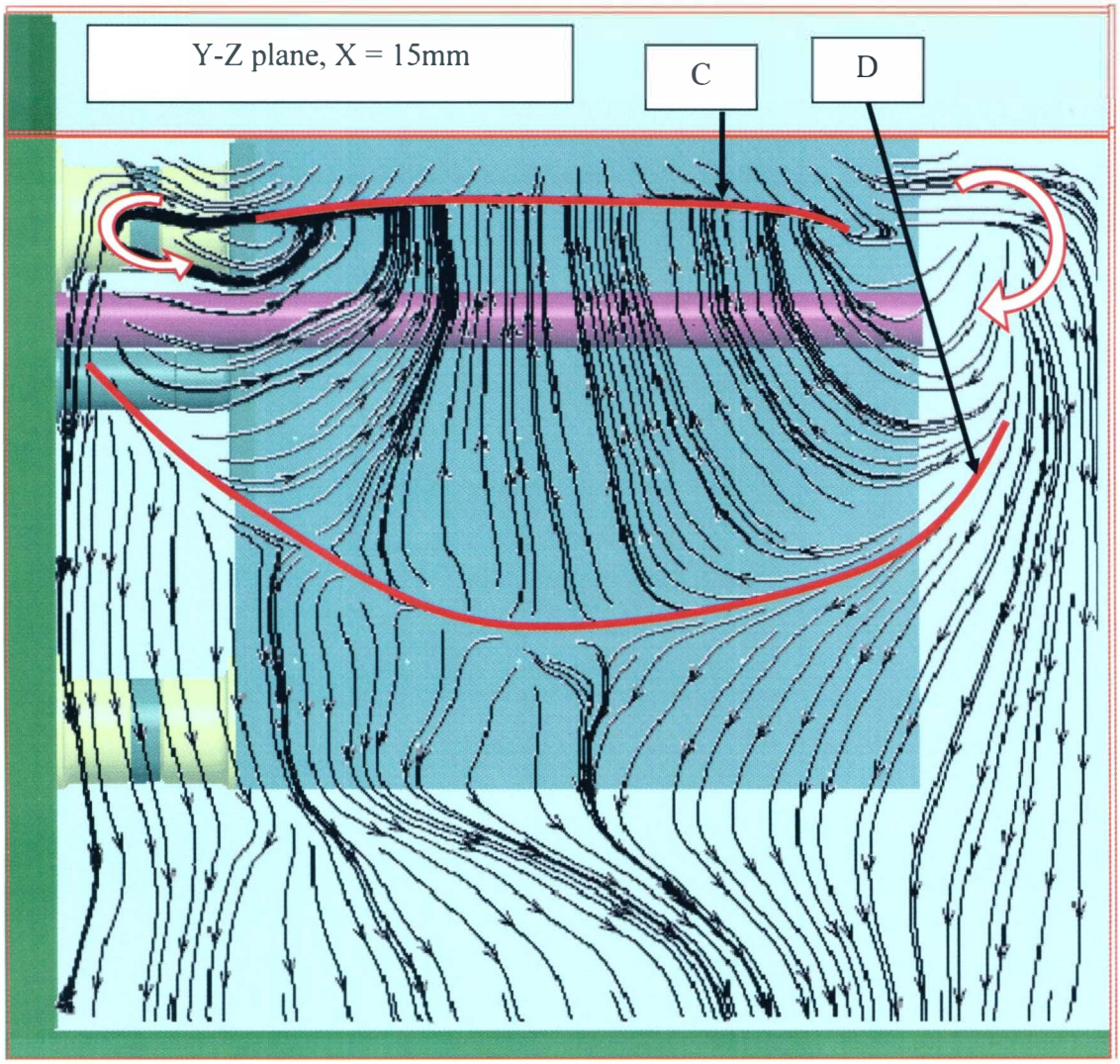

Figure 54. Velocity stream tracers of Y-Z plane at X = 15mm (left side of enclosure).

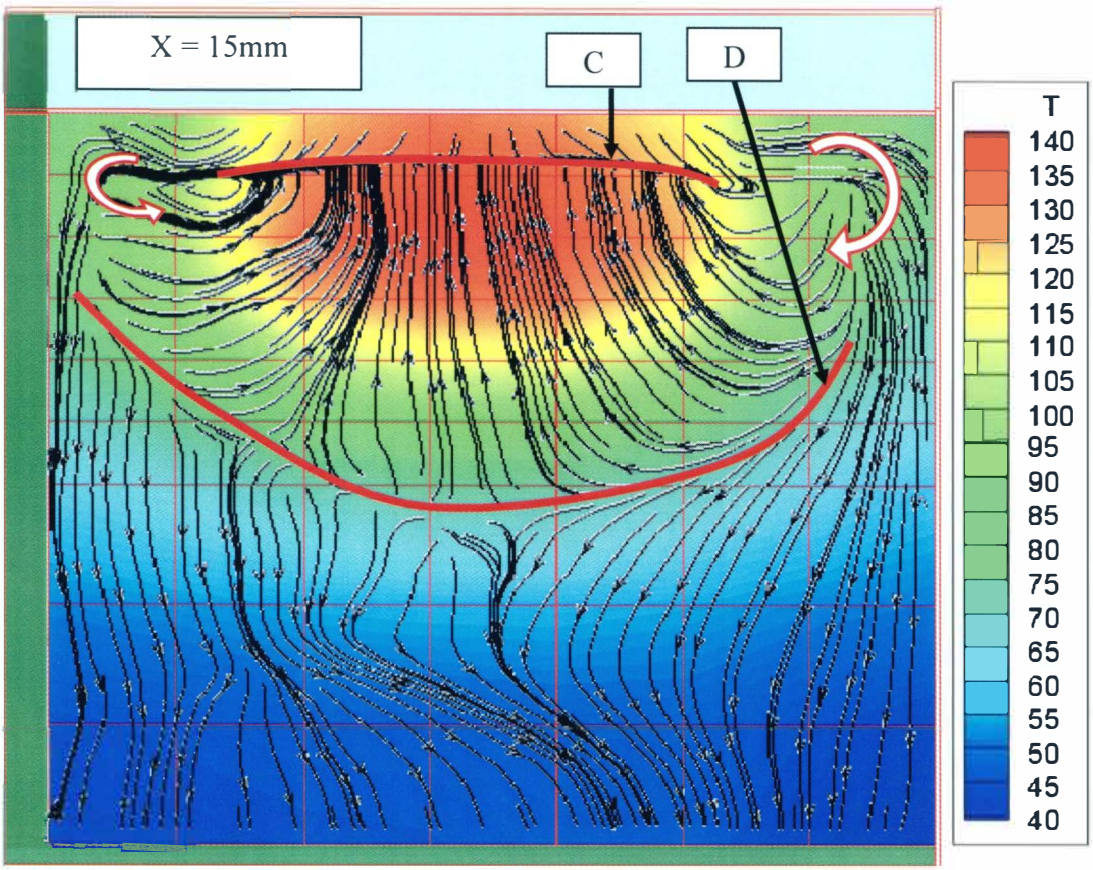

Figure 55. Velocity stream tracers of Y-Z plane at X = 15mm with left glass outer surface temperature contours.

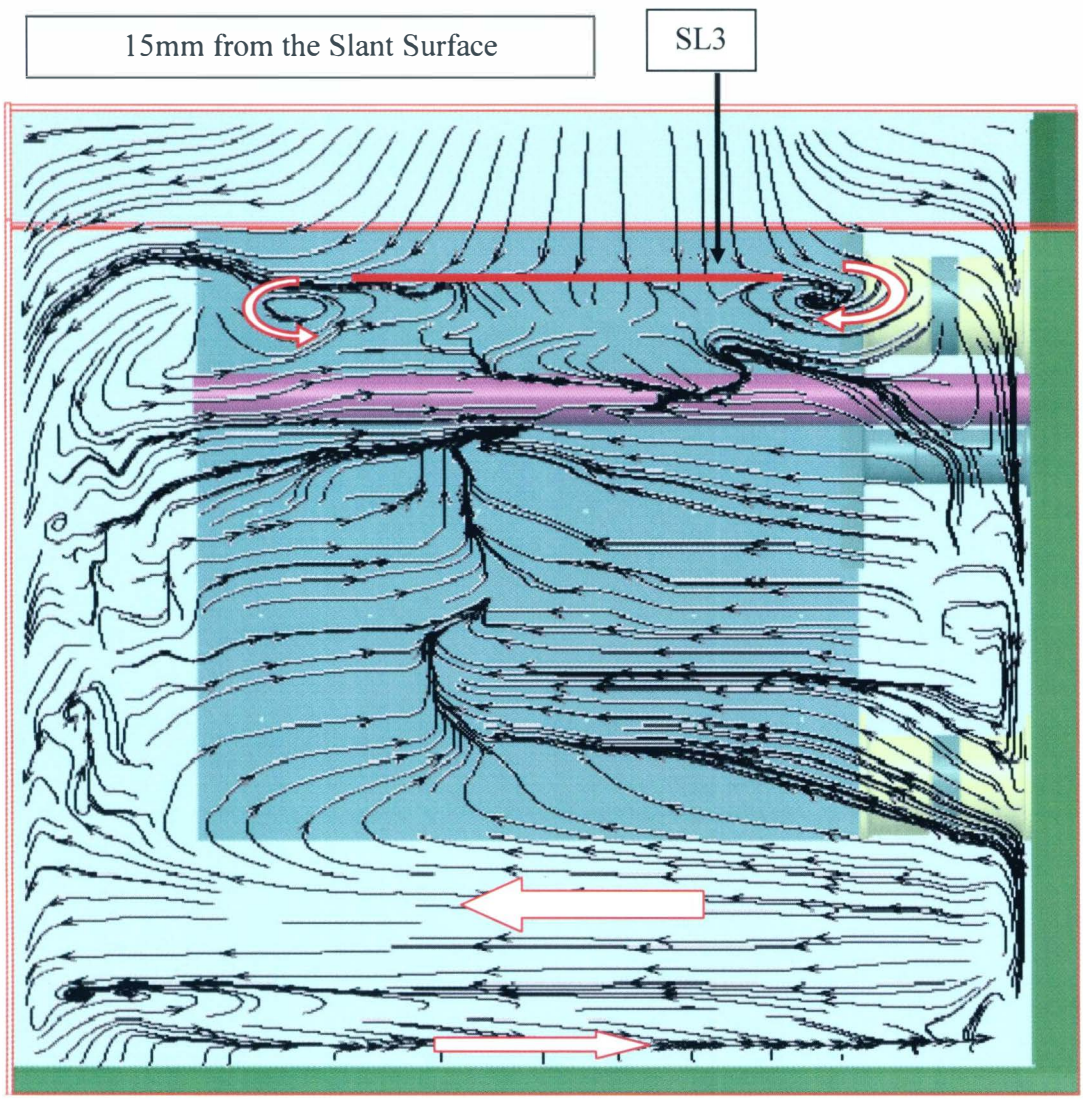

Figure 56. Velocity stream tracers of 24mm away from right slant glass surface.

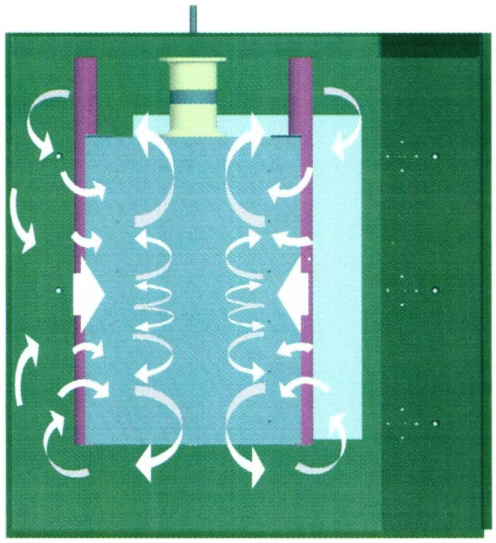

(a) Top view

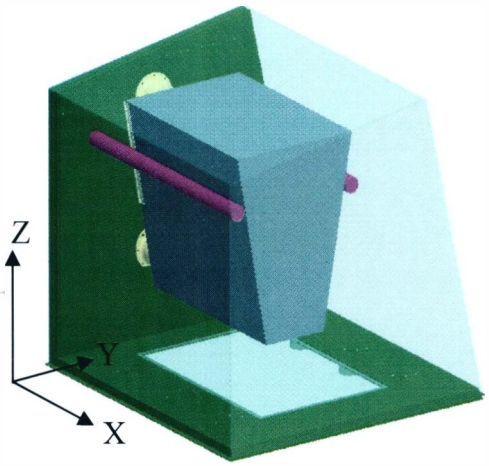

(b) Isometric view

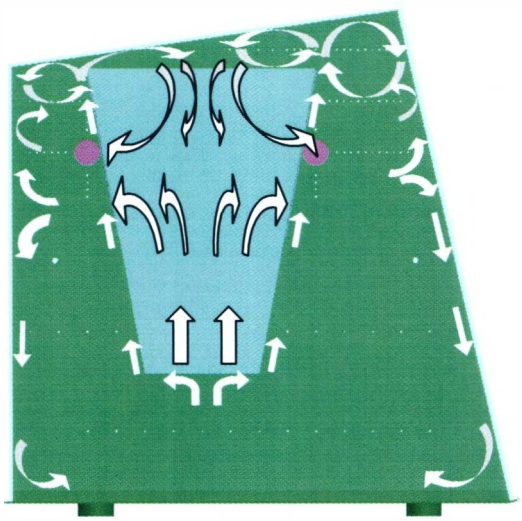

(c) Front view

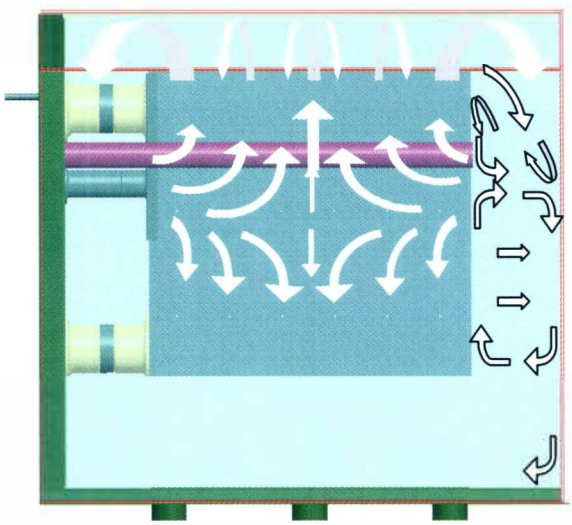

(d) Left side view

Figure 57. Interpreted main flow structures (a) Top view, (b) Isometric view, (c) Front view, (d) Left side view.

Measurement Uncertainties

Sources of error in PIV measurements are contributed by laser sheet placement, particle size consistency, and camera location. Laser sheet placement is estimated to be within $\pm$ 2mm contributed mainly by the elevation mechanism of the scissor jack cart. Inconsistency of large particle sizes effects velocity measurement at very lower velocity regions where larger particles are unable to track the flow correctly. Additionally, camera traversing mechanism has a resolution of 0.5mm to 2mm depending camera elevation on the Y-axis. Deflection from cantilevering the camera increases as it is located further from the base is unavoidable.

CHAPTER IV

CONCLUSION

The main source of heat from the exhaust heaters generates dominant flow structures on the top half of the enclosure. Highly buoyant air separates into turbulent flow after passing the top surface of the engine block due to large shear layer. Turbulent flow allows better heat transfer onto the enclosure surfaces; therefore, air temperatures are quickly reduced. Radiation from the exhaust heaters plays a dominant role in raising the temperature of the enclosure walls in the vicinity of the exhaust heaters. Complex flow and separation area are created by large temperature gradients on the enclosure walls. In this case, the top portion of the engine acts as heat sinks for air temperatures over 100 ^{o}C and side walls with temperature above 100 ^{o}C reheat the cooled air. Hence, occurrences of various flow structures are highly dependant on surface temperatures especially at close proximity between large temperature gradient surfaces and enclosure geometry. Correlating flow structures to temperature maps of the glass surfaces and air temperatures allows better understanding of the 3D flow field and also future prediction of basic flow characteristic of heated objects in an enclosure.

BIBLIOGRAPHY

[1] Merati, P., Leong, C. H., Sakuma, Y., " Investigation of the Buoyancy Driven Flow in a Simplified Full Scale Underhood- PIV and Temperature Measurements" GM Full Scale phase I report, July 13, 2006.